Transient Response of a Global Ocean–Atmosphere Model to a Doubling of Atmospheric Carbon Dioxide

SYUKURO MANABE, KIRK BRYAN AND MICHAEL J. SPELMAN

Geophysical Fluid Dynamics Laboratory/NOAA, Princeton University, Princeton, New Jersey

(Manuscript received 12 June 1989, in final form 22 November 1989)

ABSTRACT

The transient response of climate to an instantaneous increase in the atmospheric concentration of carbon dioxide has been investigated by a general circulation model of the coupled ocean–atmosphere–land system with global geography and annual mean insolation. An equilibrium climate of the coupled model is perturbed by an abrupt doubling of the atmospheric carbon dioxide. The evolution of the model climate during the 60-year period after the doubling is compared with the result from a control integration of the model without the doubling.

The increase of surface air temperature in middle and high latitudes is slower in the Southern Hemisphere than the Northern Hemisphere. The large thermal inertia of the ocean-dominated hemisphere is partly responsible for this difference.

The effective thermal inertia of the oceans becomes particularly large in high southern latitudes. Owing to the absence of meridional barriers at the latitudes of the Drake Passage, a wind-driven, deep cell of meridional circulation is maintained in the Circumpolar Ocean of the model. In addition, a deep reverse cell develops in the immediate vicinity of the Antarctic Continent. The thermal advection by these cells and associated convective overturning result in a very efficient mixing of heat in the 2-km thick upper layer and increase the effective thermal inertia of the ocean, thereby contributing to the slow down of the CO_2-induced warming of the near-surface layer of the Circumpolar Ocean of the model.

It is surprising that, during the last 15 years of the 60-year experiment, sea surface temperatures in the Circumpolar Ocean actually reduce with time. Because of the increase in precipitation caused by the enhanced penetration of warm, moisture-rich air aloft into high latitudes, the surface halocline of the Circumpolar Ocean intensifies, thereby suppressing the convective mixing between the surface layer and the warmer underlying water. Thus, sea surface temperature is reduced in the Circumpolar Ocean towards the end of the experiment.

In the Northern Hemisphere, the CO_2-induced warming of the lower troposphere increases with increasing latitudes and is at a maximum near the North Pole due partly to the albedo feedback process involving sea ice and snow cover. The warming of the upper ocean layer also increases with increasing latitudes up to about 65°N where the absorption of solar radiation increases markedly due to the poleward retreat of sea ice. Over the Arctic Ocean, the warming is very large in the surface layer of the model atmosphere, whereas it is very small in the underlying water. Both sea ice and a stable surface halocline act as thermal insulators and are responsible for the large air–sea contrast of the warming in this region.

In short, the CO_2-induced warming of the sea surface has a large interhemispheric asymmetry, in qualitative agreement with the results from a previous study conducted by use of a coupled model with a sector computational domain and an idealized geography. This asymmetry induces an atmospheric response which is quite different between the two hemispheres.

1. Introduction

The transient response of climate to the future increases of greenhouse gases is receiving increased attention. Early studies on this topic (e.g., Hoffert et al. 1980; Cess and Goldenburg 1981; Hansen et al. 1984) discussed the delay of the response due to the thermal inertial of the oceans. However, the models used for these studies have highly idealized oceanic components that do not explicitly incorporate the effect of heat transport by ocean currents. Therefore, the horizontal distribution of the transient climate response was not discussed in these studies. The present study represents an attempt to do this by use of a coupled ocean–atmosphere model in which the effect of both advection and convective overturning in the oceans are explicitly taken into consideration.

Bryan et al. (1982) started the investigation of this problem using a simple, coupled ocean–atmosphere model. For computational economy and ease of analysis, their model had a one-hemisphere, sector computational domain bounded by the equator and two meridians, which are 120° longitude apart. Symmetry is assumed at the equator and cyclic continuity is imposed at the meridional boundaries. To provide a large signal-to-noise ratio, the equilibrium climate of the

Corresponding author address: Dr. Syukuro Manabe, Geophysical Fluid Dynamics Laboratory, Princeton University, P.O. Box 308, Princeton, NJ 08542.

model was perturbed by an abrupt four-fold increase of atmospheric carbon dioxide. They found that 25 years after the abrupt quadrupling of carbon dioxide, the latitudinal profile of the transient response of surface air temperature is qualitatively similar to the equilibrium response of surface air temperature. For example, the tendency towards the polar amplification found in the equilibrium response study also appears in this transient response. Sea ice and the polar halocline effectively insulate the atmosphere from the deep ocean and allow a large change in surface air temperature near the pole.

Schlesinger et al. (1985) investigated the response of their coupled ocean–atmosphere model to an abrupt doubling of atmospheric carbon dioxide. The increase of zonal mean surface air temperature becomes larger with increasing latitudes, in qualitative agreement with the result of Bryan et al. (1982), and is nearly symmetric relative to the equator.

Thompson and Schneider (1982) concluded that the qualitative similarity between the transient and equilibrium responses in the result of Bryan et al. (1982) is attributable to the idealized geography of the model used. They noted that the Southern Hemisphere, which is covered mostly by oceans with large thermal inertia, should respond more slowly than the Northern Hemisphere.

Responding to the critique of Thompson and Schneider, Bryan et al. (1988) again investigated the transient response of climate using a modified version of their model. The sector computational domain of the original model was extended from one to two hemispheres. The ratio of land to sea at each latitude corresponds to the actual land–sea ratio for the present geography of the earth. At the latitudes of the Drake Passage, the entire sector is occupied by ocean.

They analyzed the evolution of this coupled system during the 50 years following an abrupt doubling of atmospheric carbon dioxide. In the Northern Hemisphere, the increase of surface air temperature became larger with increasing latitudes in qualitative agreement with the results of earlier studies. However, the response of surface air temperature in the Southern Hemisphere lagged substantially behind the response in the Northern Hemisphere. In particular, it was surprising that surface air temperature did not increase at all in high latitudes in the Southern Hemisphere. Bryan et al. concluded that this large interhemispheric asymmetry in the response of surface air temperature was attributable to the following factors. One is the large oceanic fraction of the Southern Hemisphere noted by Thompson and Schneider. Another is the upwelling of deep water in the Circumpolar Ocean, which prevents sea surface temperature from rising significantly around the Antarctic Continent.

The simple sector geography model constructed by Bryan et al. was useful for getting a preliminary idea of the physical processes involved in the transient response of the coupled ocean atmosphere system. However, it is desirable to evaluate their results using a coupled model with a global computational domain and a more realistic geography. The present study represents an attempt to do this using the global model developed at the Geophysical Fluid Dynamics Laboratory of NOAA.

The structure and performance of this global model were recently described by Manabe and Stouffer (1988). Because of the systematic bias of this model towards suppressing the thermohaline circulation and exaggerating the surface halocline in the North Atlantic Ocean, the air–sea exchange of water was adjusted to remove this bias. With this adjustment the simulated structure of the coupled ocean–atmosphere system is sufficiently realistic to warrant using this model to study the sensitivity and transient response of climate.

For the present study, the atmospheric concentration of carbon dioxide is doubled abruptly. Since a given curve of growth may be approximated by superposition of step functions, it was originally hoped that the results from the present experiment might be used to compute the response of the coupled model to a more realistic, gradual increase of atmospheric carbon dioxide. However, this assumption is not justified because the response of the coupled system is a nonlinear function of the CO_2-forcing. Fortunately, the abrupt doubling of atmospheric carbon dioxide assumed in the present study induced a relatively quick response of the coupled model and facilitated the identification and analysis of the basic physical mechanisms involved in the CO_2-induced change of climate.

2. The coupled model

The coupled ocean–atmosphere model used for this study consists of a general circulation model of the World Ocean coupled to a general circulation model of the atmosphere. Heat and water budgets of the continental surface are included. The model has a global domain, realistic geography and annually averaged insolation. Figure 1 is a box diagram which illustrates the basic components of the model and how they interact.

In the atmospheric component of the model, the dynamic computation is performed using a spectral transform method in which the horizontal distribution of a predicted variable is represented by a truncated series of spherical harmonics and grid point values (Gordon and Stern 1982). The resolution is limited by a cutoff beyond zonal wave number 15. The same number of degrees of freedom is used in representing the latitudinal distribution of each zonal wave component. The effects of clouds, water vapor, carbon dioxide, and ozone are included in the calculation of solar and terrestrial radiation. The distribution of water vapor is predicted in the model, but the mixing ratio of carbon dioxide is assumed to be constant in the

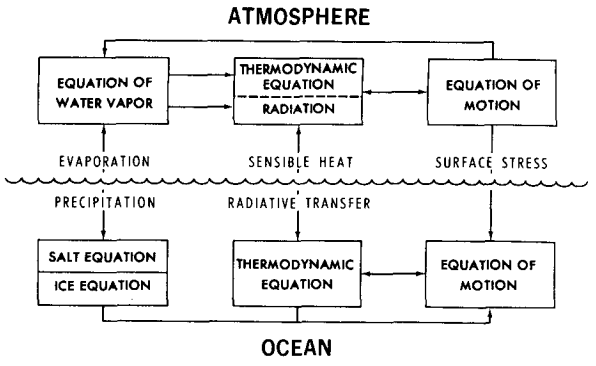

FIG. 1. Components of the ocean-atmosphere climate model (from Manabe and Bryan 1969).

model atmosphere. Ozone is specified as a function of latitude and height from observations. The annually averaged values of height, thickness and fractional amount of cloud cover are also specified, in reference to the results of London (1957) and Sasamori and London (1972). Another major simplification of the model is the specification of solar radiation without seasonal variation. The solar constant is assumed to be 1353 W m^{-2}.

Precipitation is simulated whenever supersaturation is indicated by the prognostic equation for water vapor. The precipitation is identified as snowfall when the air temperature near the surface falls below freezing; otherwise it is identified as rain. Moist convective processes are parameterized by a moist convective adjustment scheme as described in Manabe et al. (1965).

The computation of land surface temperature satisfies the constraint of no surface heat storage. That is, the contributions from net fluxes of solar and terrestrial radiation and turbulent fluxes of sensible and latent heat must balance locally. The albedo distribution of snow-free surfaces is determined by referring to the study of Posey and Clapp (1964). When the surface is covered by snow, the albedo is replaced by a higher value depending on surface temperature and snow depth. For deep snow (water equivalent at least 2 cm), the surface albedo is 60% if the surface temperature is below −10°C and 45% at 0°C, with a linear interpolation between these values from −10° to 0°C. When the water equivalent of the snow depth is less than 2 cm, it is assumed that the albedo decreases from the deep snow values to the albedo of the underlying surface as a square root function of snow depth.

The change in snow depth is computed as the net contribution of snowfall, sublimation and snowmelt which is determined from the requirement of surface heat balance (see Manabe 1969, for further details).

The budget of soil moisture is computed by the so-called bucket method (Manabe 1969). Within the model, soil is assumed to have the ability to contain 15 cm of liquid water. When soil is not saturated with water, the change of soil moisture is predicted as the net contribution of rainfall, evaporation and snowmelt. If the soil moisture value reaches the field capacity of 15 cm, the excess water is regarded as runoff. The rate of evaporation from the soil surface is determined as a function of the water content of the "bucket" and potential evaporation, i.e., the hypothetical evaporation rate from a completely wet surface.

The oceanic component of the model is similar to the model described by Bryan and Lewis (1979). The primitive equations of motion are constructed by use of Boussinesq, rigid-lid and hydrostatic approximations. Subgrid scale motion is included as turbulent viscosity or turbulent diffusion. Whenever the vertical stratification in the model oceans is unstable, it is assumed that the coefficient of vertical diffusion becomes infinitely large, and the vertical gradients of both temperature and salinity are removed. This process of convective adjustment together with the large scale sinking of dense water contributes to the formation of deep water in the model oceans.

The finite difference mesh of the oceanic component of the model has a spacing between grid points of 4.5° latitude and 3.75° longitude. It has 12 levels for the finite differencing in the vertical direction. The computational resolution specified above is marginally adequate for representing coastal currents but cannot describe mesoscale eddies.

The bathymetry of the model is shown in Fig. 2. Because of the coarse computational resolution, many features of the bottom topography are only crudely resolved. For example, the mid-Atlantic Ridge of the model is not as high above the sea floor as observed; also Iceland is eliminated. To resolve computationally the ocean currents passing through the narrow Drake Passage, the meridional span of the passage in the upper oceanic layers is expanded to four grid intervals, i.e., 2000 km. No attempt is made to resolve the flow through the Strait of Gibraltar. Instead, the water at the westernmost Mediterranean grid point is mixed horizontally and completely with the water at the adjacent Atlantic grid point to a depth of 1350 meters.

The prognostic system of sea ice is similar to the very simple free drift model developed by Bryan (1969). The sea ice moves freely with the surface ocean currents provided that its thickness is less than 4 m, but is stationary for higher values. Following Broccoli and Manabe (1987), the albedo of sea ice depends on surface temperature and ice thickness. For thick sea ice (at least 1 m thick), the surface albedo is 80% if the surface temperature is below −10°C and 55% at 0°C, with a linear interpolation between these values for intermediate temperatures. If the ice thickness is less than 1 m, the albedo decreases with a square root function of ice thickness from the thick ice values to the albedo of the underlying water surface.

As indicated in Fig. 1, the atmospheric and oceanic components interact with each other through ex-

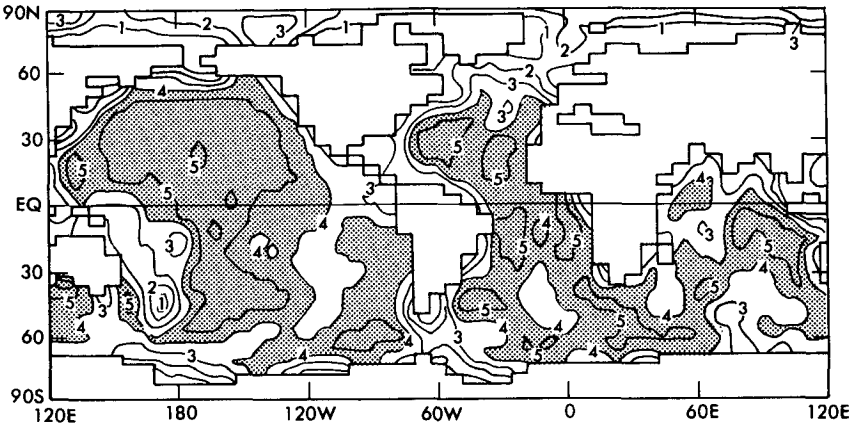

FIG. 2. The smoothed topography of the ocean model. Depths are given in kilometers.

changes of heat, water, and momentum. The heat exchange is accomplished by the net radiative flux and turbulent fluxes of sensible and latent heat. The water (or ice) exchange consists of evaporation (or sublimation), rainfall (or snowfall), and runoff from the continents. The runoff flows in the direction of steepest descent based on the specified topography. Glacier flow is computed in a similar manner. To prevent indefinite growth of an ice sheet through snow accumulation, it is assumed that the water equivalent depth of snow does not exceed 20 cm and the excess snow also runs off by glacial flow in the direction of the steepest descent and instantly reaches the oceans. The ocean surface temperature and sea ice predicted in the ocean are used as lower boundary conditions for the atmosphere. Details of the heat, moisture, and momentum exchange processes are given, for example, by Manabe (1969).

3. Equilibrium state

In order to simulate the transient response of climate to an increase of atmospheric carbon dioxide, it is desirable to obtain an equilibrium state of the model as an initial condition for a transient response experiment. When the time integration of a model is initiated from a nonequilibrium state, it exhibits a rapid drift of the model climate towards its equilibrium. As the CO_2-concentration in the model atmosphere begins to increase, such a drift is superposed upon the CO_2-induced change of the model climate, making the interpretation of the experimental results very difficult. Therefore, the equilibrium state of the model was computed as a preparation for the transient response experiment described in section 4. This section describes briefly the procedure used for the time integration of the coupled model described in the preceding section, followed by the description of the equilibrium state of the model. For further details of these topics, see the recent study of Manabe and Stouffer (1988), who explored the structures of the stable equilibria of the coupled model.

a. Asynchronous time integration

To reduce the computer time needed to reach the equilibrium state of the coupled model, an asynchronous method of time integration (Manabe and Bryan 1969; Manabe 1969) was performed. In this time integration method, the evolution of the oceanic component of the model with large thermal inertia was accelerated by a factor of approximately 150. Thus, an 8-year integration of the atmospheric component of the model was performed concurrently with a 1250-year integration of the oceanic component, continuously exchanging information on the interfacial interaction between the atmosphere and oceans of the model. The approach of the temperature and salinity in deeper ocean layers towards the equilibrium values is accelerated further as described by Bryan et al. (1975) and Bryan (1984), thereby extending the effective length of the time integration to 34 000 years. Towards the end of this asynchronous integration, there was no systematic trend in the temporal variation of global mean sea surface temperature. This suggests that the model climate is close to an equilibrium state.

As pointed out in the Introduction, the asynchronous integration of the coupled model as described above yields an unrealistic distribution of surface salinity, particularly over the northern North Atlantic where an unrealistically intense halocline develops and the formation of deep water is suppressed. A discussion of the factors responsible for the bias of the present model toward the halocline catastrophe is contained in Manabe and Stouffer (1988). (See the final paragraph of the concluding section of their paper.) To prevent this halocline catastrophe, the exchange of water between the atmospheric and oceanic components of the model is continuously adjusted throughout the course of the integration, counterbalancing the systematic bias of the model. This adjustment varies geographically but is constant with time. Depending upon the initial conditions chosen, two different equilibria emerged. When

the time integration starts from a realistic initial condition, the distribution of salinity remains realistic and the thermohaline circulation is maintained in the North Atlantic Ocean throughout the course of the integration. On the other hand, when it starts from a simple initial condition of an isothermal ocean with a constant salinity overlain by an isothermal atmosphere, an extremely intense halocline develops in the northern North Atlantic despite the water flux adjustment mentioned above, completely suppressing the thermohaline circulation in the Atlantic Ocean. Both equilibria mentioned above are described in detail by Manabe and Stouffer. Since the former solution with more realistic water mass structure is used for the transient response experiment conducted in the present study, it will be described briefly in the following subsection.

b. *Description of quasi-equilibrium*

This subsection briefly describes the quasi-equilibrium state, which is identified above and is used for the transient response experiment as described in section 4. Figure 3 compares the horizontal distribution of the time-mean sea surface temperature of the coupled model to the observed distribution compiled by Levitus (1982). This comparison indicates that the computed sea surface temperature in the northern North Atlantic is slightly colder than the observed. In the Circumpolar Ocean of the Southern Hemisphere, the region where sea surface temperature is below zero is narrower in the computed than in the observed pattern, indicating a slight overestimate of the sea surface temperature in this region. In low latitudes, the general values of simulated sea surface temperature coincide approximately with those of the observed. Although there are many differences between the two distributions in Fig. 3, the general characteristics of sea surface temperature are reproduced reasonably well.

The latitude–depth distribution of zonal mean temperature in the model oceans is compared with the observed distribution in Fig. 4. In general, the simulated thermocline is significantly deeper than the observed. This result suggests that the model may overestimate the downward penetration of the thermal anomaly that occurs in response to an increase of atmospheric carbon dioxide. One should keep in mind this unrealistic be-

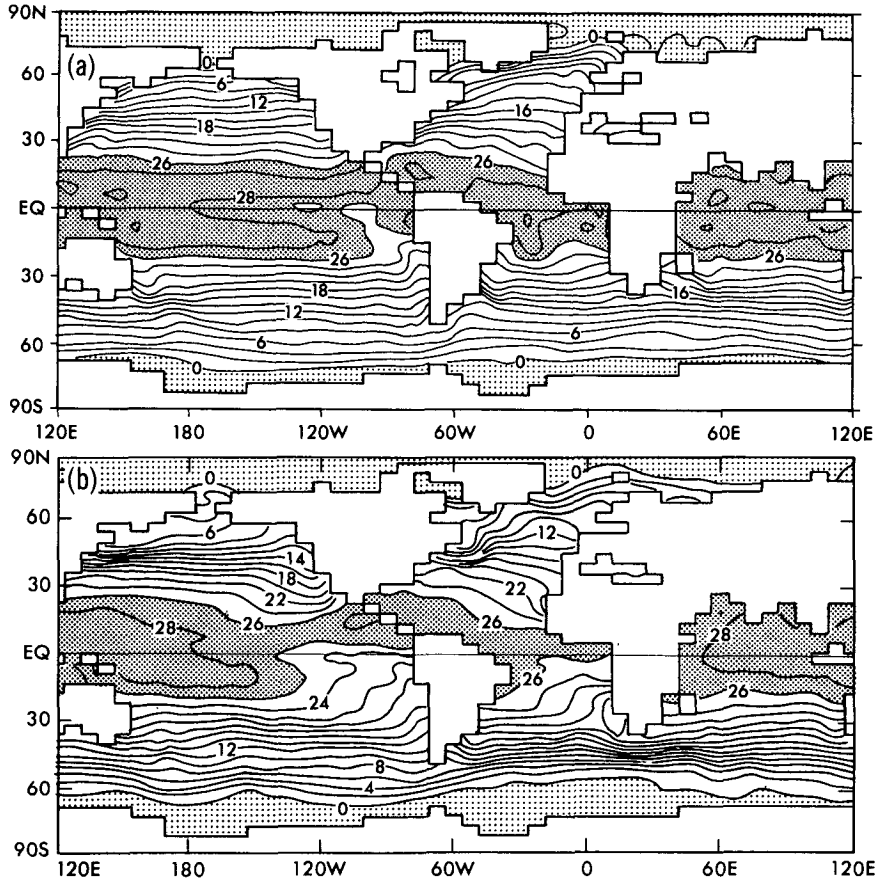

FIG. 3. Annually averaged sea surface temperature in degrees Celsius: (a) computed for the equilibrium climate with normal atmospheric carbon dioxide content; (b) observed (Levitus 1982).

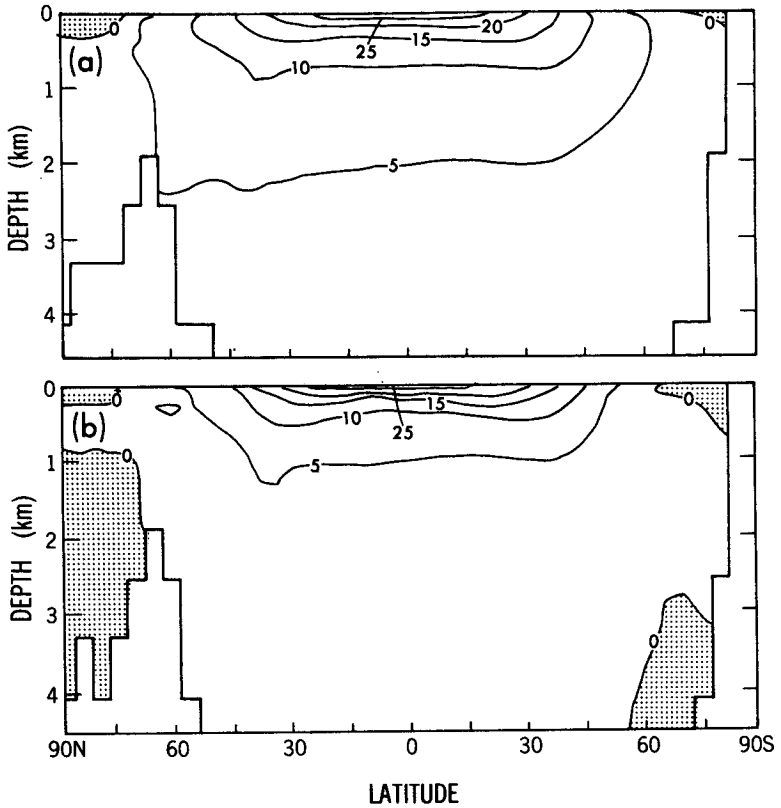

FIG. 4. Depth distribution of zonally averaged temperature: (a) computed for the equilibrium climate with normal atmospheric carbon dioxide content; (b) observed (Levitus 1982). Units are degrees Celsius.

havior of the present model when interpreting the results from the transient response experiment described in section 4. Although it is not evident in Fig. 4, the global mean bottom water temperature of the model ocean is about 4°C and is higher than the observed, which is about 1°C. This warm bias of the model may result partly from the fact that the present model with annual mean insolation misses the winter season when saline surface water generated by the formation of sea ice sinks and lowers the temperature of the bottom water in various oceans, e.g., the coastal region of the Antarctic Continent.

The geographical distribution of the time-mean surface air temperature is compared with the observed distribution (Crutcher and Meserve 1970) in Fig. 5. This figure indicates that the surface air temperature in the model tropics is slightly lower than the observed. Other notable discrepancies between the computed and the observed distributions include the model's overestimation of several degrees Celsius along the Antarctic coast where the thickness and coverage of sea ice are underestimated. On the other hand, the surface air temperature over the Arctic region is similar to the observed. The thermal ridges along the west coast of Europe and North America are reproduced very well. In general, the characteristics of the simulated distribution of surface air temperature resemble very closely those of the observed distribution.

Owing to the surface water flux adjustment described above, the geographical distribution of surface salinity is similar to observations, and therefore, is not shown here. Figure 6 compares the latitude–depth distributions of simulated and observed zonal mean salinities beneath the surface. Although the simulated distribution shown in Fig. 6a misses the downward and northward intrusion of the salinity minimum indicative of Antarctic Intermediate Water, it exhibits many of the features of the observed distribution shown in Fig. 6b. For example, the model successfully simulates a shallow Arctic halocline, the downward penetration of the salty water attributable to the existence of the Mediterranean water and the near-surface salinity maximum in the subtropics of the Southern Hemisphere. Although it is obscured by the zonal averaging procedure, the downward and southward penetration of fresh intermediate water in the Northern Pacific is also reproduced by the model. In general, the effective depth of the downward penetration of the simulated surface salinity pattern appears to be more realistic than the depth of the simulated thermocline discussed above.

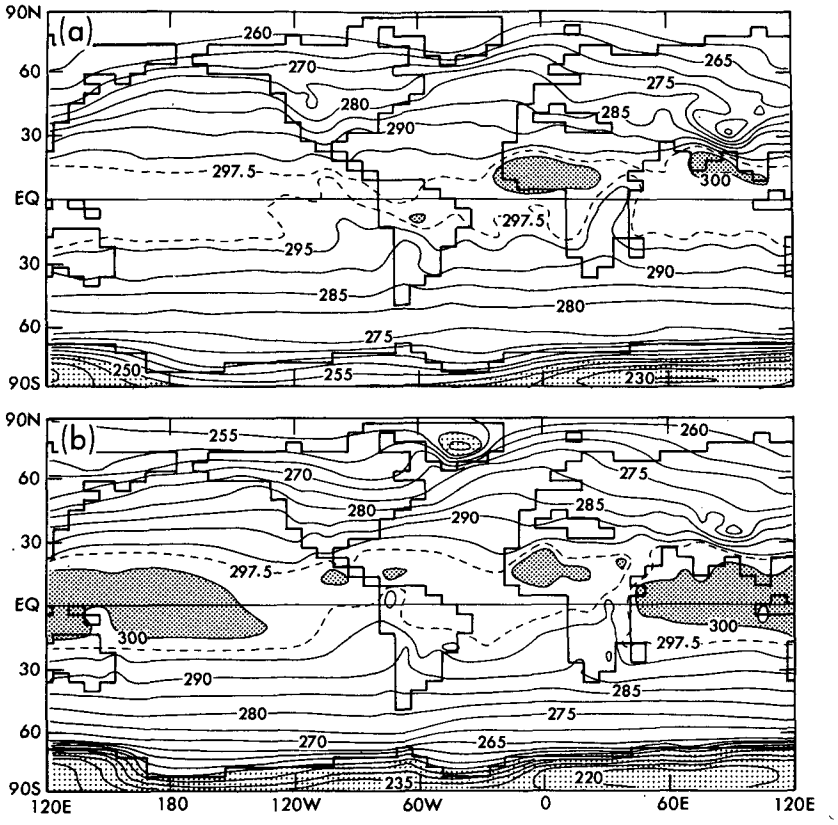

FIG. 5. Annually averaged surface air temperature in degrees Kelvin: (a) computed for the equilibrium climate with normal carbon dioxide content; (b) observed (Crutcher and Meserve 1970; Taljaard et al. 1969).

The streamfunction of zonally integrated, time mean meridional circulation in both atmosphere and oceans of the model is illustrated in Fig. 7. Considering the interfacial stress and the balance of forces in the atmospheric and oceanic Ekman layers, it is reasonable that the Ekman transport in the atmosphere is directed in the opposite direction from that in the oceans of the model. At around 50°S latitude, one can identify a deep, anticlockwise oceanic cell, which underlies the atmospheric Ferrel cell. As explained in section 5, the deep, downward penetration of this wind-driven cell is due to the absence of a meridional barrier at the latitudes of the Drake Passage. Although it is weaker, there is another clockwise cell in the coastal ocean of the Antarctic Continent. It will be shown later that the vertical thermal advection by these cells and associated convective overturning delay the warming of the near-surface layer in the Circumpolar Ocean of the Southern Hemisphere.

As noted in the explanation of the time integration procedures in section 3, the model maintains the thermohaline circulation in the North Atlantic Ocean. This circulation appears in the streamfunction of Fig. 7 as a cell with a sinking branch at about 60°N and a rising branch in low latitudes.

c. *Equilibrium response*

Before discussing the transient response of the coupled model to the abrupt doubling of atmospheric carbon dioxide, it is useful to determine the equilibrium response, i.e., the total response achievable over an infinite length of time. By comparing the transient response with the equilibrium response, one can assess the degree of the thermal adjustment of the coupled system towards the equilibrium state with the higher CO_2 concentration.

The preceding section describes how the so-called asynchronous time integration procedure was used to obtain the equilibrium state with the normal CO_2 concentration. The same method was also used to get another equilibrium that has twice the normal amount of CO_2. Throughout both time integrations, an identical water flux adjustment, described in section 3, was performed. The equilibrium response was computed as the difference between the two equilibria.

The latitude–height distribution of the equilibrium response of the zonal mean temperature to the CO_2 doubling is illustrated in Fig. 8. This figure indicates that the warming of the lower troposphere due to the doubling increases with increasing latitudes in both

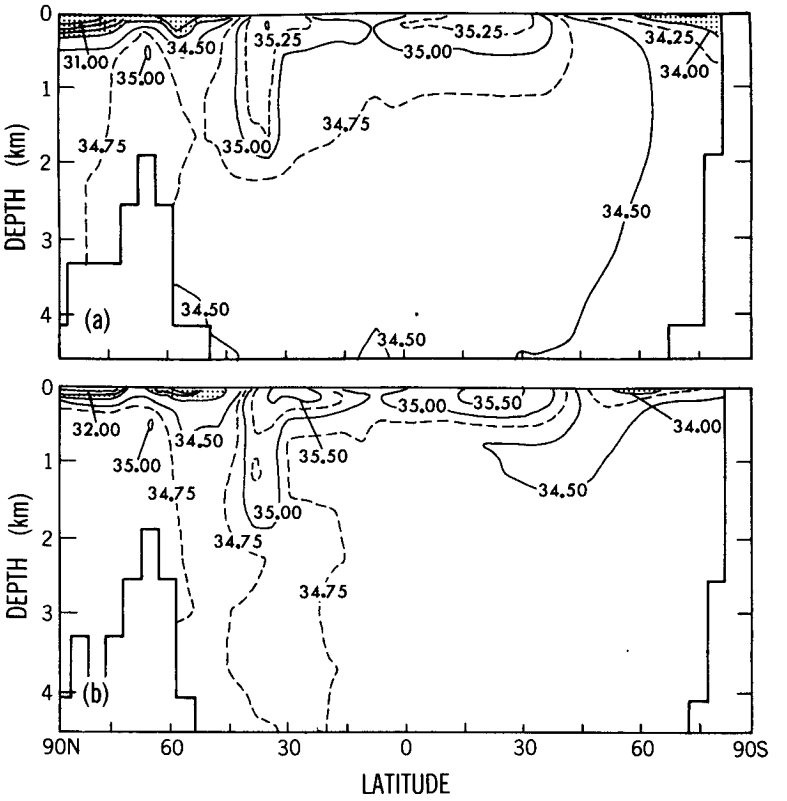

FIG. 6. Depth distribution of zonally averaged salinity: (a) computed for the equilibrium climate with normal atmospheric carbon dioxide content; (b) observed (Levitus 1982). Units are parts per thousand.

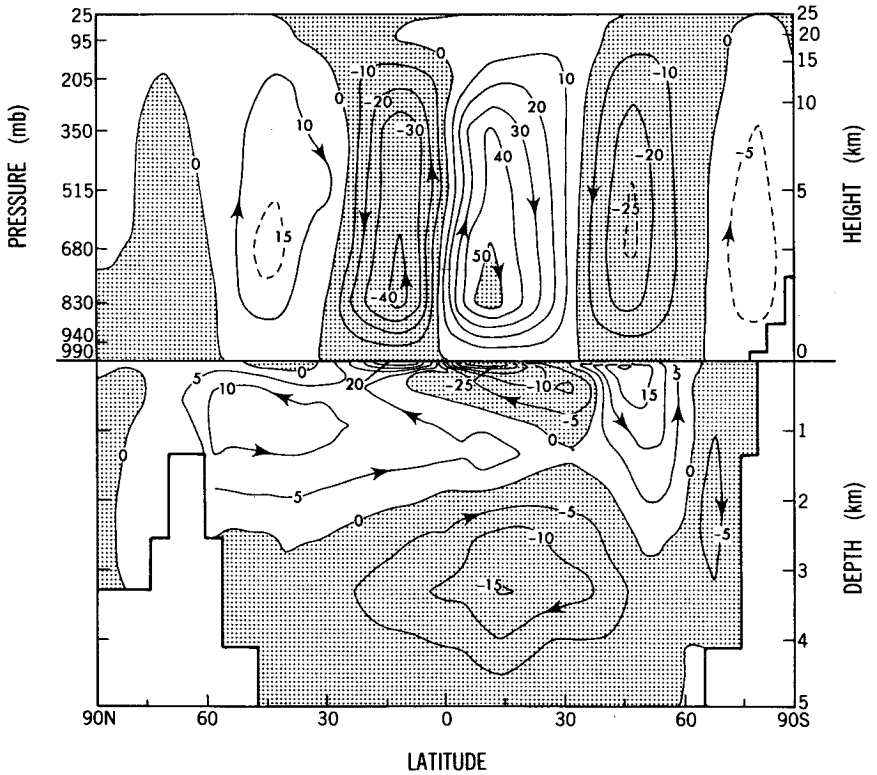

FIG. 7. Zonally integrated mass transport of the atmosphere and ocean for the equilibrium climate with normal atmospheric carbon dioxide content. Units are megatons/sec.

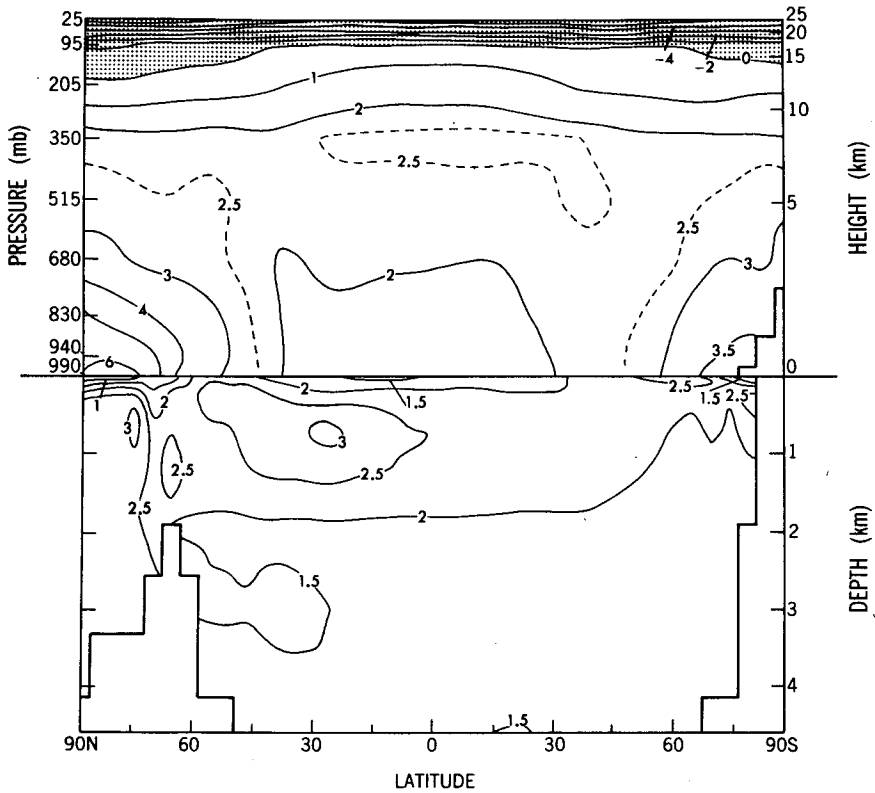

FIG. 8. Zonally averaged temperature response of the atmosphere and ocean for the equilibrium climate for the doubling of atmospheric carbon dioxide. Units are degrees Celsius.

hemispheres and is at a maximum in the two polar regions. This polar amplification in the equilibrium response of the lower tropospheric temperature results partly from the positive feedback process involving snow and sea ice with high surface albedo. It is also attributable to the very stable stratification of the lower model troposphere to which the polar warming is confined. The damping of such a near-surface temperature anomaly by the longwave radiation into space is small, helping to sustain the large polar warming.

Averaged over an entire hemisphere, the difference in surface air temperature between the two equilibria in the Northern and Southern hemispheres is 2.5° and 2.3°C, respectively. Since the warming of the model troposphere is nearly symmetric relative to the equator, as indicated by Fig. 8, it is reasonable that these values are comparable with each other. This equilibrium response of the coupled model is in sharp contrast to its transient response, which has a marked interhemispheric asymmetry as discussed in the following section.

In the model oceans, the near-surface warming increases with latitude up to about 55°N (or S) from where it reduces towards the polar regions. Because the thermal insulation due to sea ice and the stable halocline prevent vertical mixing, the warming of near-surface water in the polar region remains small despite the very large warming of the overlying air in the polar regions.

Figure 8 indicates that the CO_2-induced warming of equilibrium temperature below a depth of 2 km is smaller than the warming above that depth. This is attributable to the fact that the intensity of the North Atlantic thermohaline circulation in the high CO_2 case is about 60% of its intensity in the normal CO_2 case. Thus, the warming of the deep Atlantic layer due to advection and convection is smaller in the high CO_2 atmosphere. Warm moisture-rich air penetrates into higher latitudes, increasing precipitation over the Arctic and surrounding oceans and developing a more intense halocline, thereby weakening the thermohaline circulation in the North Atlantic Ocean.

4. Transient response experiment

a. Temperature and salinity variations

To investigate the transient response of the coupled ocean–atmosphere model to a doubling of atmospheric carbon dioxide, two synchronous integrations of the model were conducted. In the first integration the normal concentration of the atmospheric carbon dioxide was specified. This synchronous integration, which starts from the end of the asynchronous integration

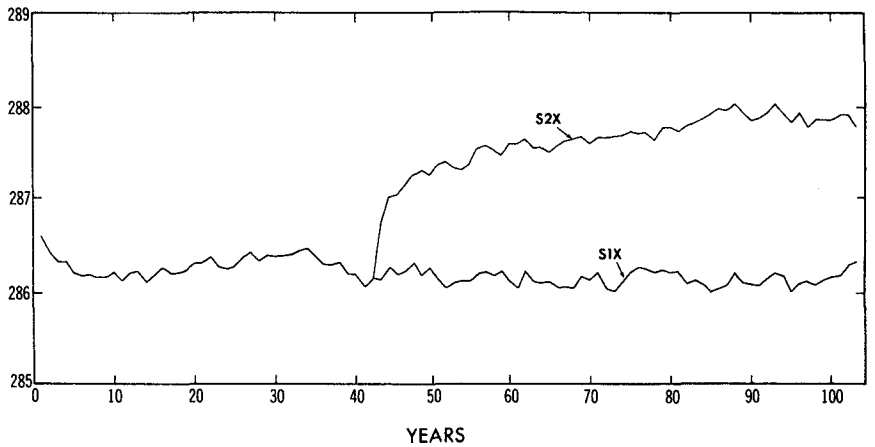

FIG. 9. Globally averaged annual mean surface air temperature (degrees Kelvin) as a function of time for the synchronous integrations. The curve labeled S1X represents the control run with normal atmospheric carbon dioxide content; S2X represents the experiment in which the atmospheric carbon dioxide is doubled.

described in the preceding section, was performed over a period of 102 model years. From the 42nd year of this first integration, the second synchronous integration was started. The atmospheric concentration of carbon dioxide was doubled abruptly at the beginning of the second integration and remained constant during the following 60-year period. Hereafter, the first and the second integrations mentioned above will be called the S1X and S2X integrations, respectively. By examining the difference between these two integrations, the influence of an abrupt CO_2 doubling upon the state of the coupled model was investigated.

Figure 9 illustrates the temporal variations of the control and response integrations mentioned above. According to this figure, the global mean surface air temperature has no systematic trend during the last 60 year period of the control (S1X) integration. In the second (S2X) integration, the global mean surface air temperature becomes higher than the control integration following the CO_2 doubling. For the convenience

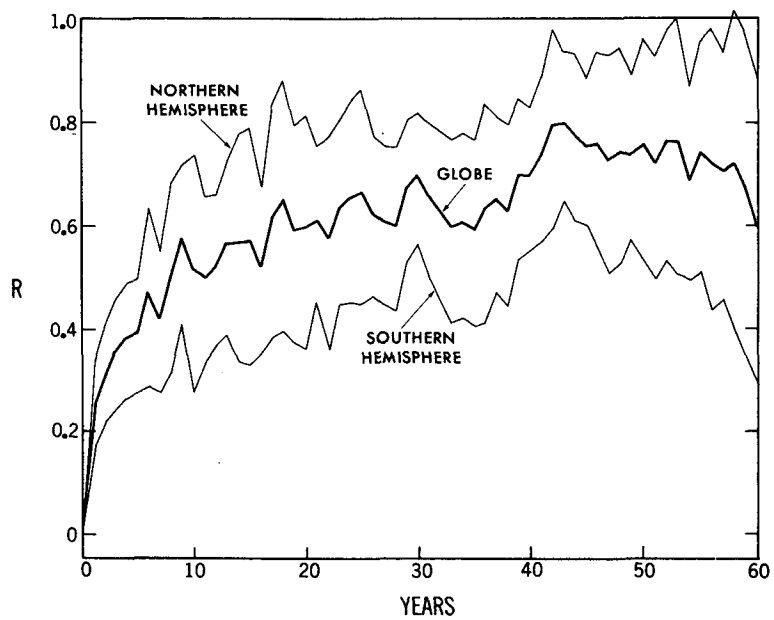

FIG. 10. The transient response of annually averaged surface air temperature as a function of time for the synchronous integration shown separately for the Northern Hemisphere, globe, and Southern Hemisphere. The response, R, is the temperature change for the doubling of carbon dioxide normalized by the equilibrium temperature change.

of comparison, it is assumed hereafter that the time lines of both integrations start when the second integration branches off from the control. In this new chronology, both integrations start in the 0th year and end in the 60th year. The temporal variation of the difference between the two integrations during this 60-year overlapping period represents the response of the model to the abrupt doubling of atmospheric carbon dioxide.

As an indicator of the approach towards the destination, i.e., the equilibrium state of the model with twice the normal CO_2 concentration, a quantity $\mathcal{R}_A$ is defined by

$$\mathcal{R}_A \equiv \frac{(\overline{T_a^{S2X}(t)})^A - (\overline{T_a^{S1X}(t)})^A}{(\overline{T_a^{2Xe}})^A - (\overline{T_a^{1Xe}})^A}$$

where T_a^{S1X} and T_a^{S2X} denote the surface air temperature obtained from the S1X and S2X integrations; t is the time elapsed from the beginning of the 60-year period. The T_a^{1Xe} and T_a^{2Xe} are equilibrium surface air temperatures for the normal and twice normal CO_2 concentration in the model atmosphere, and $(\overline{\ })^A$ denotes area-averaging over domain A, which is chosen to be the Northern Hemisphere, the Southern Hemisphere, or the entire globe. Figure 10 illustrates the temporal variations of $\mathcal{R}_A$ computed for these three domains. According to this figure, the response of surface air temperature in the Southern Hemisphere lags substantially behind that in the Northern Hemisphere. It is surprising that the warming in the Southern Hemisphere reaches the peak around the 43rd year of the integration and decreases with time thereafter. This decrease during the final period of the integration is the subject of a later discussion.

Figure 11a illustrates how the latitudinal distribution of the difference in zonal mean surface air temperature between the two integrations changes with time. This

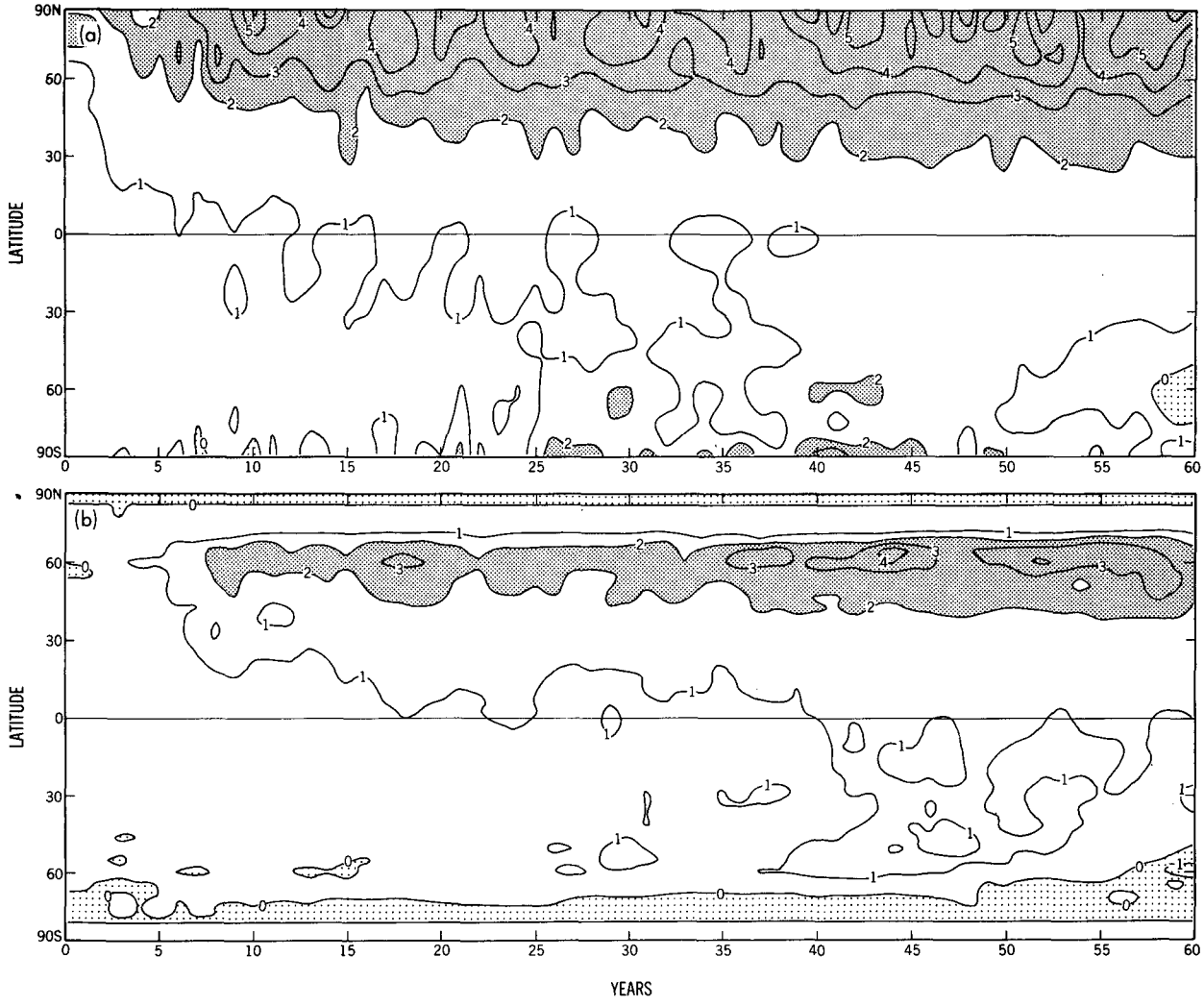

FIG. 11. Zonally averaged annual mean temperature change (degrees Celsius) as a function of latitude and time for the doubling of atmospheric carbon dioxide: (a) surface air temperature; (b) sea surface temperature.

figure again indicates a large interhemispheric asymmetry in the CO_2-induced warming. In the Northern Hemisphere of the model, the warming proceeds at a much faster pace than in the Southern Hemisphere and is at a maximum over the Arctic Ocean. A similar polar amplification of the warming is not evident in the Southern Hemisphere. Instead, the warming in high latitudes increases at a much slower rate than in the Northern Hemisphere and begins to decrease with time at around the 45th year. This is consistent with the temporal variations of hemispheric mean surface air temperatures shown in Fig. 10. It is surprising that around the 60th year, a small region of net cooling appears around 60°S latitude.

The zonal mean sea surface temperature difference shown in Fig. 11b also exhibits a large interhemispheric asymmetry, though the warming is at a maximum around 60°N from where it is reduced towards the Arctic Ocean covered by sea ice. In the Southern Hemisphere, the warming is smaller. It is notable that the sea ice-covered zones of no warming around the Antarctic Continent expand northward after the 50th year of the integration.

Accompanying the change in sea surface temperature described above, sea ice thickness also undergoes significant change during the 60-year period. Figure 12 illustrates the temporal variation of the difference in zonal mean sea ice thickness between the S2X and S1X integrations. Over the Arctic Ocean of the model, sea ice in the S2X integration becomes thinner as compared with the S1X integration. The CO_2-induced reduction of sea ice thickness is at a maximum around 60° ~ 70°N latitude where the sea ice margin retreats poleward, inducing a large warming of the sea surface, as indicated in Fig. 11b. In contrast to the situation in the Arctic Ocean, the CO_2-induced change of zonal mean sea ice thickness in the coastal seas around the Antarctic Continent is usually positive and increases with time. One notes, however, the significant reduction in zonal mean sea ice thickness at about 60°S latitude, i.e., along the northern margin of sea ice during the 20th to 50th year period. These changes in zonal mean sea ice thickness are consistent with the changes in sea surface temperature shown in Fig. 11b.

The temporal and latitudinal variation of the difference in zonal mean surface salinity between the S2X and S1X integrations is illustrated in Fig. 13. This figure indicates that in the polar oceans of both hemispheres, the difference in zonal mean surface salinity is reduced during the 60-year period of the experiment. For example, the salinity of the surface mixed layer of the Arctic Ocean becomes substantially smaller in the S2X as compared with the S1X integration. In the surface mixed layer of the Southern Hemisphere, the zonal mean salinity difference between the two integrations is also reduced even though it did so at a much slower pace. The rate of reduction accelerated somewhat during the last 15-year period (i.e., 45 ~ 60th year). As discussed later, these reductions in both polar oceans are triggered by the increased surface water flux, enhanced further by an accompanying change in oceanic circulation.

The geographical distribution of the difference in surface air temperature between the two integrations is illustrated in Fig. 14a. The corresponding distribution of sea surface temperature difference is added as Fig. 14b. These distributions represent the averages over the 10-year period from the 50th to 60th year. In general, these figures are consistent with the latitudinal profiles of zonal mean temperature difference described above. They indicate that the positive difference in surface air temperature is particularly large near the Sea

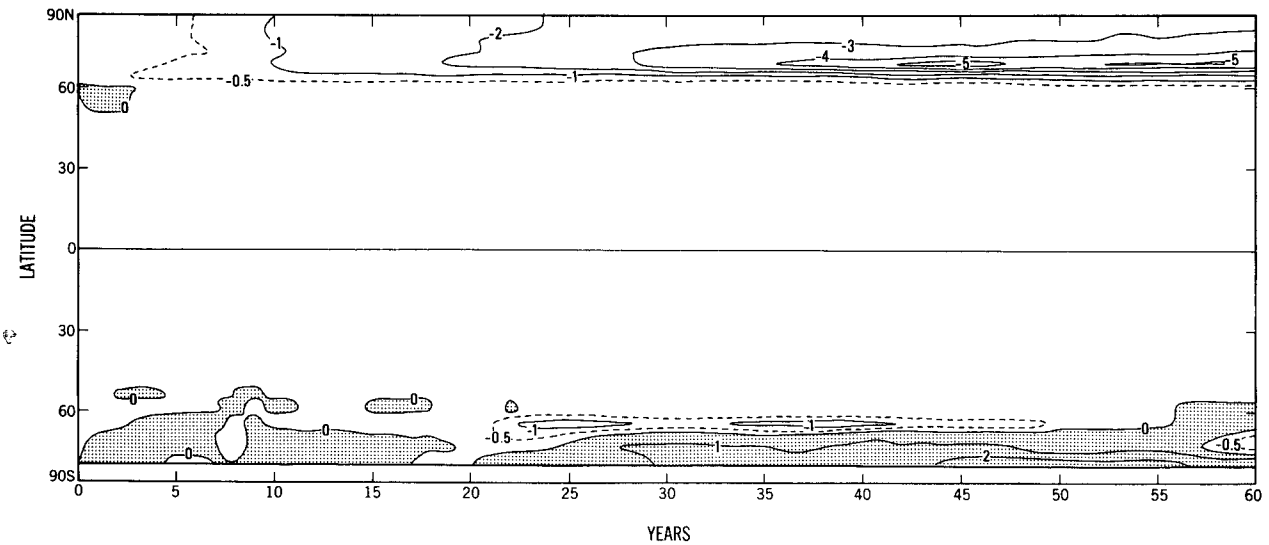

FIG. 12. Zonally averaged change of annual mean sea ice thickness (meters) as a function of latitude and time for the doubling of atmospheric carbon dioxide.

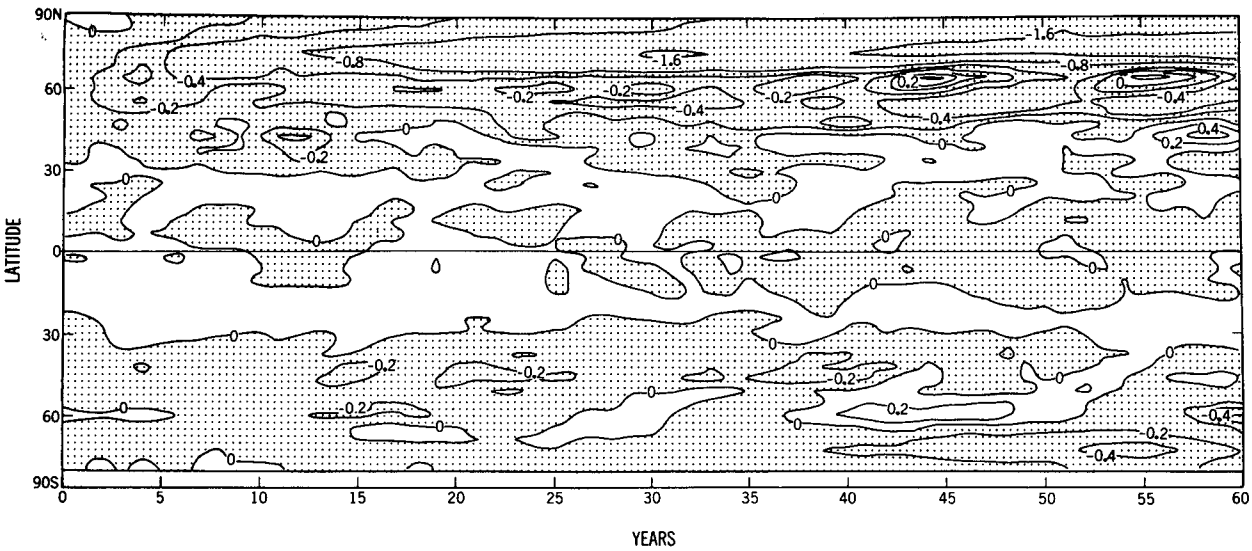

FIG. 13. Zonally averaged annual mean ocean salinity change (parts per thousand) at the surface as a function of latitude and time for the doubling of atmospheric carbon dioxide.

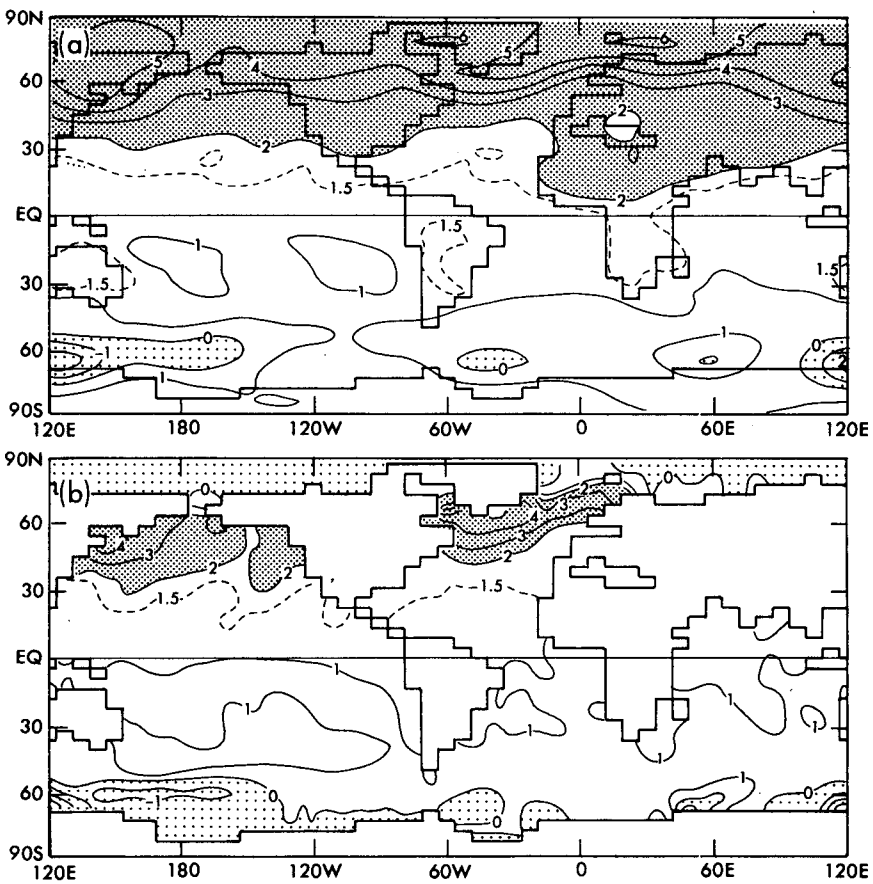

FIG. 14. Temperature difference (degrees Celsius) between the doubling and normal atmospheric carbon dioxide climates, averaged for the period 50 to 60 years of the synchronous integration (a) surface air temperature difference; (b) sea surface temperature difference.

of Okhotsk and the Greenland Sea. The rise of sea surface temperature is also pronounced in these regions. For example, it is at a maximum in the northwestern sectors of both the Atlantic and Pacific oceans. In the Southern Hemisphere, the differences in both surface air- and sea surface temperatures decrease with increasing latitudes and become even negative in several regions along the coast of the Antarctic continent.

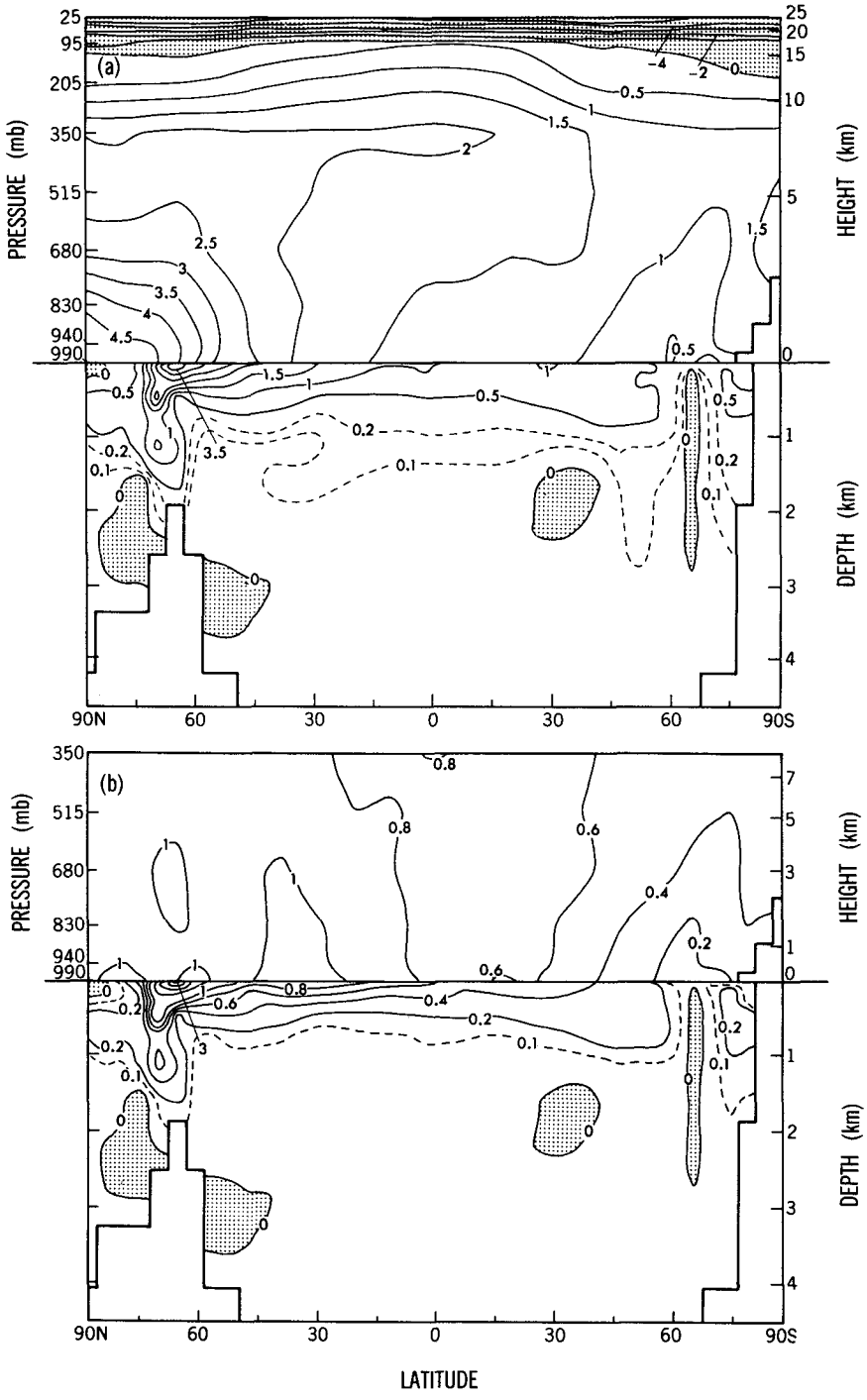

FIG. 15. Zonally averaged temperature response of the atmosphere and ocean for the doubling of atmospheric carbon dioxide: (a) transient response in degrees Celsius averaged over the period 50 to 60 years of the synchronous integration; (b) normalized response corresponding to the transient response in (a) divided by the equilibrium response shown in Fig. 8.

To evaluate the vertical as well as latitudinal distribution of the CO_2 warming, the difference in zonal mean temperature between the two integrations is averaged over the 10-year period from the 50th to 60th years and is illustrated as a function of latitude and height (or depth) in Fig. 15a. Again, one notes a large interhemispheric asymmetry in this distribution. For example, the difference in the zonal mean temperature of the lower troposphere is at a maximum over the Arctic, decreases towards the south, and becomes small over and around the Antarctic Continent. In the upper model troposphere, the difference is again larger in the Northern than the Southern Hemisphere. However, its interhemispheric asymmetry is less.

In the model oceans, the downward penetration of the warm anomaly is essentially confined to the upper layers. The warming in the Northern Hemisphere increases with increasing latitudes, is at a maximum from 50° to 75°N, and becomes small over the Arctic Ocean where sea ice insulates the upper ocean layer from the near surface layer of the atmosphere with large warming.

In the Circumpolar Ocean of the Southern Hemisphere, the warming is small, particularly in the 50° ~ 75°S belt, in sharp contrast to the situation in the Northern Hemisphere. Around 65°S latitude, there exists even a narrow column of small negative temperature change. The warming is no more than several tenths degrees Celsius in the subsurface layer of the coastal region of the Antarctic Continent.

The transient response of zonal mean temperature shown in Fig. 15a may be evaluated in light of the equilibrium response shown in Fig. 8. As was done earlier with respect to hemispheric mean surface temperature, the ratio of the transient response of zonal mean temperature to the equilibrium response is computed. This ratio should be useful for evaluating how far the model atmosphere has approached towards the equilibrium response, which is the response to be achieved over an infinite length of time. Figure 15b illustrates the latitude–height (or depth) distribution of this ratio. The ratio is not shown in the upper troposphere and stratosphere of the model because it cannot be determined around the tropopause where the denominator is very close to zero. This figure indicates that, in most of the troposphere of the Northern Hemisphere, this ratio exceeds 0.8, whereas it is as small as 0.2 over the Circumpolar Ocean of the Southern Hemisphere. In the upper layers of the model oceans, the ratio is relatively large and decreases southwards from 65°N to 65°S latitude. However, it is close to zero in the Arctic Ocean and is very small in the coastal region of the Antarctic continent. The ratio is also very close to zero in the deeper layers of the model oceans.

The distribution of the CO_2-induced warming of the coupled system in the Northern Hemisphere is qualitatively similar to the result which was obtained by Bryan et al. (1982) from their ocean–atmosphere model with a sector computational domain confined to one hemisphere. Both results indicate a polar amplification by the CO_2-induced warming of the lower model troposphere, which is caused by the positive albedo feedback effect of sea-ice and snow cover. Because of the thermal insulation by sea-ice and the halocline surrounding it, the warming of the lower troposphere continued over the Arctic Ocean despite the absence of warming in the deeper ocean layers (Spelman and Manabe 1984).

b. Heat budget of the coupled system

To evaluate the radiation budget of the coupled ocean–atmosphere system, the zonal mean differences in radiative fluxes between the S2X and S1X integrations are computed at the top of the model atmosphere and are time-averaged over the entire 60-year period of the experiment. Figure 16 illustrates the latitudinal profiles of the differences in the net fluxes of solar and terrestrial and total radiation. In this figure, the positive and negative differences indicate the net gain and loss of radiation energy by the coupled system which occurred in response to the doubling of atmospheric carbon dioxide.

In the zonal belt ranging from 30°N and 55°S latitudes, the net incoming solar radiation increases by about 0.3 W m^{-2} because the reflected solar radiation is reduced due to the increased absorption of solar energy by the atmosphere with higher moisture content. In the same latitude belt, the coupled system gains heat by about 0.8 W m^{-2} because of the reduction of heat loss by the outgoing terrestrial radiation. The increase

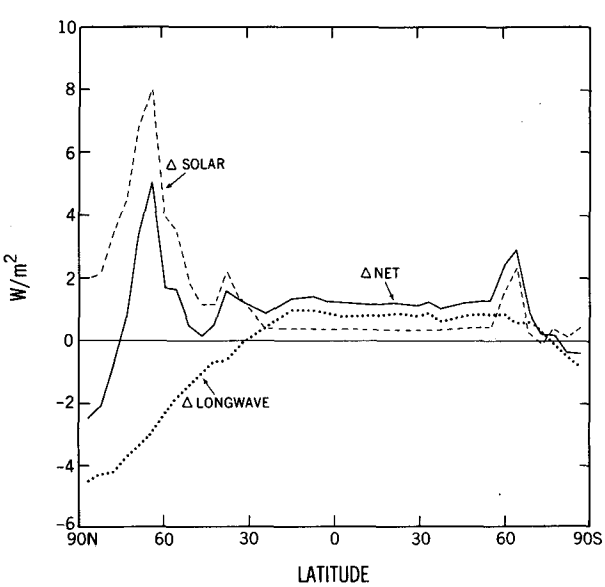

FIG. 16. Zonally averaged change of the radiation at the top of the atmosphere for the doubling of atmospheric carbon dioxide, averaged over the entire 60 years of the model integration. Positive difference represents net heat gain for the coupled model. Units are W m^{-2}.

in the atmospheric concentrations of carbon dioxide and water vapor raises the altitude, and lowers the temperature, of the effective source of emission for the outgoing terrestrial radiation at the top of the atmosphere. Thus, the changes in both solar and terrestrial fluxes of radiation sum up to the heat gain of about 1.2 W m^{-2} in the 30°N ~ 50°S belt, contributing to the warming of the coupled system throughout the course of the experiment.

Figure 16 also indicates that, in high latitudes of the Northern Hemisphere, the coupled system gains heat due to the increase in the net downward flux of solar radiation. The increase of surface air temperature caused by the doubling of atmospheric carbon dioxide results in the poleward retreat of sea ice and snow cover with large surface albedos, thereby enhancing the absorption of incoming solar radiation and increasing the net incoming solar radiation at the top of the model atmosphere. This increase far exceeds the increase of the outgoing terrestrial radiation which results mainly from the large warming of surface and overlying air in high northern latitudes. The net gain of radiational energy is mostly absorbed by the model oceans, thereby contributing to the relatively large warming of the model oceans around 40° ~ 70°N latitudes as shown in the preceding subsection.

The time mean heat budget of a vertical water column of the ocean for the duration of the experiment may be expressed by the following equation:

$$\frac{1}{t_F}\left[\left(C\int_0^D T\rho dD\right)^{t=t_F} - \left(C\int_0^D T\rho dD\right)^{t=0}\right] = \frac{1}{t_F}\int_0^{t_F} Q_s dt + \overline{\mathrm{ADV}} + \overline{\mathrm{DIF}} \quad (1)$$

where T, C, and ρ are temperature, heat capacity and density of water, respectively. D is depth, t is time, t_F is the time of the termination of the experiment (i.e., 60th year in the present experiment), Q_s is the heat supply at the ocean surface and $\overline{\mathrm{ADV}}$ + $\overline{\mathrm{DIF}}$ are the time mean contributions of advection and subgrid-scale diffusion to the heat budget. For the sake of simplicity, the change in the negative latent heat stored in sea ice is neglected here.

The rate of change of the oceanic heat content as defined by the left-hand side of equation (1) is computed for both S2X and S1X integrations. The difference in the time mean rate of heat content change between the two integrations is zonally averaged over the oceanic segment of a latitude circle and is compared with the corresponding difference in time averaged, zonal mean ocean surface heat flux in Fig. 17a. The former represents the time mean rate of CO_2-induced oceanic heat storage and the latter is CO_2-induced change in surface heat flux averaged over the duration of the experiment. To explore the heat budget of a latitude belt, these quantities are multiplied by the length of the oceanic segment of a latitude belt and are illustrated in the lower half of the figure (i.e., Fig. 17b).

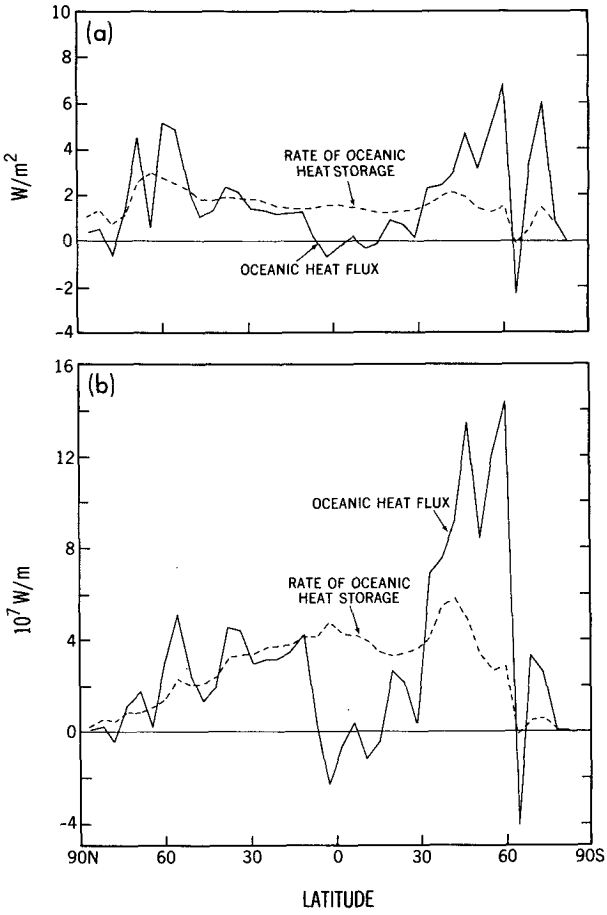

FIG. 17. (a) Zonally averaged components of the heat balance of the ocean for the doubling of atmospheric carbon dioxide, averaged over the entire 60 years of the model integration. Units are W m^{-2}; (b) the components in (a) multiplied by the length of the oceanic segment of each latitude belt, in units of 10^7 W m^{-1}.

Figure 17a shows that, when the heat content per unit oceanic area is considered, the increase in the rate of heat storage in middle and high latitudes of the Southern Hemisphere is somewhat smaller than that in the Northern Hemisphere. However, when the heat content is integrated over the entire oceanic portion of a latitude belt (Fig. 17b), the former is substantially larger than the latter because a larger fraction of the area is covered by oceans in the Southern Hemisphere. In agreement with the suggestion of Thompson and Schneider (1982), these results indicate that the slower increase of sea surface temperature in middle and high latitudes of the Southern Hemisphere is partly attributable to the larger thermal inertia of the wider oceans.

However, there are *other important mechanisms* which can reduce the rate of the warming in the high southern latitudes. As noted already in the preceding subsection, the sea surface temperature in middle and

high latitudes of the Southern Hemisphere increases at a substantially slower rate than the Northern Hemisphere counterpart. Accordingly, the surface heat loss due to evaporation, sensible heat flux, and radiative emission is reduced markedly, accounting for the very large net heat gain (i.e., positive change in oceanic surface heat flux) in middle and high latitudes of the Southern Hemisphere. This CO_2-induced surface heat gain far exceeds the corresponding increase in the rate of oceanic heat storage in the 30°–60°S latitudes as Fig. 17 indicates. On the other hand, the reverse is the case in low latitudes where the evaporative heat loss from the oceanic surface increases due to the enhanced subsidence of dry air. These results imply that, in response to the CO_2 doubling, the oceanic heat transport changes in such a way to transfer heat from the middle to low latitudes of the Southern Hemisphere. In short, the increase of the temperature of the upper ocean layer in middle and high latitudes of the Southern Hemisphere is slow not only due to the preponderance of oceans with large thermal inertia but also due to the enhanced net export of heat by ocean currents. As discussed in the following section, there exists, however, an important mechanism that is mainly responsible for the very slow rise of sea surface temperature in the Circumpolar Ocean of the Southern Hemisphere.

c. *Circumpolar Ocean*

In this subsection, it is shown that the absence of significant surface warming in the Circumpolar Ocean of the Southern Hemisphere is mainly attributable to the deep cells of meridional circulation and associated convection in the Circumpolar Ocean. According to Fig. 7, which illustrates the meridional circulation in the model ocean, a deep anticlockwise cell underlies the atmospheric Ferrel Cell around latitude 50°S. Although it is weaker, another clockwise oceanic cell exists in the coastal region of the Antarctic Continent. As discussed below, the thermal advection by these cells and associated convective overturning results in a very effective mixing of heat in a thick oceanic layer, thereby delaying the warming of the Circumpolar Ocean surface.

The deep cell under the middle latitude westerlies in the Southern Hemisphere owes its existence to the absence of a meridional barrier at the Drake Passage. Bryan et al. (1988) investigated this issue by use of a coupled ocean–atmosphere model with a sector computational domain bounded by two meridians 120° longitude apart and an idealized geography. They compared the results from two versions of the model with and without a meridional barrier at the Drake Passage. In the version with the closed Drake Passage, a zonal pressure gradient develops and southward geostrophic flow prevails just below the northward Ekman drift current as noted by Gill and Bryan (1971). However, in the version without the meridional barrier, the zonal pressure gradient is small. Thus, the westerly-induced equatorward Ekman drift can only be compensated by a deep downwelling north of the Drake Passage gap, southward geostrophic flow at the base of the gap, and deep upwelling south of the Circumpolar current. In summary, the existence of this deep cell is attributable in large part to the existence of the gap between South America and Antarctica and the prevalence of intense westerlies at the latitude of the Drake Passage. The presence of deep-water upwelling south of the Circumpolar current has been suggested based upon the analysis of water mass structure (Deacon 1937; Sverdrup et al. 1942). Because of its poor computational resolution, the present model may not incorporate the effect of bottom topography upon the circulation at the latitudes of the Drake Passage. It is encouraging, however, that a deep wind-driven cell has been simulated also by a high resolution model (Semtner and Chervin 1988).

To evaluate how the heat budget of water in the Circumpolar Ocean is maintained, various terms of the thermodynamical equation computed for both S2X and S1X integrations are analyzed in the Circumpolar Ocean. For the convenience of discussion, the thermodynamical equation is written as

$$\frac{\partial T}{\partial t} = \text{ADV} + \text{CONV} + \text{DIF} + \text{SQ}$$

where $\partial T/\partial t$ denotes the rate of net temperature change, the advection term ADV contains the contributions from both horizontal and vertical components, CONV represents the effect of convective overturning, DIF contains the contributions from both vertical and horizontal subgrid scale diffusion, and SQ is the net heating of the ocean mixed layer due to the net incoming radiation, sensible and latent heat fluxes from the surface, and the freezing and melting of sea ice. For both S1X and S2X integrations, each term in the thermodynamical equation is time-averaged for the entire 60 year period and is area-averaged over the model oceans polewards of 50°S. Figure 18a illustrates the vertical distribution of ADV, CONV, DIF and SQ in the subsurface layer (i.e., the layer below 295 m) from the S1X integration. The differences of these terms between the two integrations are shown as a function of depth in Fig. 18b.

These figures indicate that the influence of both advection and convection penetrate deeply into the Circumpolar Ocean. As Fig. 7 shows, there are two deep cells of meridional circulation in middle and high latitudes of the Southern Hemisphere. In the 40°–60°S latitudes, there is a wind-driven deep cell, which was discussed extensively in this section. With the exception of the oceanic mixed layer, whose heat budget is maintained in a quite different manner, the thermal advection by this cell warms the upper ocean layer to a depth of approximately 2 km. On the other hand, the con-

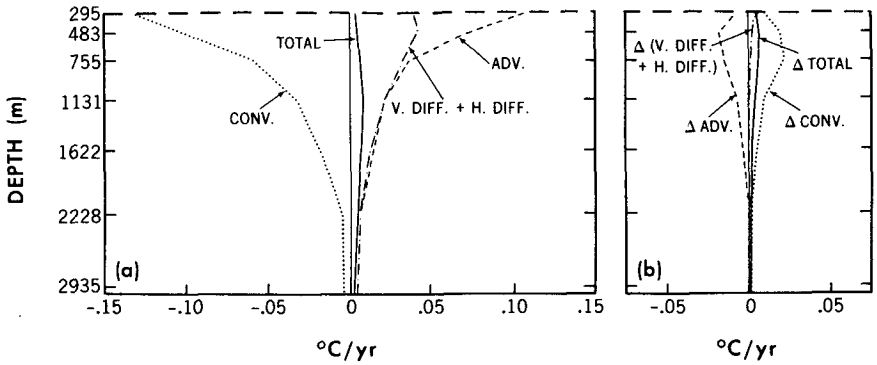

FIG. 18. Components of the rate of temperature change in the model ocean between 295 and 3000 m depth, averaged over the area from 50°S to the coast of the Antarctic Continent for the entire 60 years of integration: (a) the synchronous integration with normal atmospheric carbon dioxide; (b) the difference between the integrations with doubled and normal carbon dioxide. The components of the rate of temperature change are advection (denoted ADV), convection (CONV), and combined horizontal and vertical diffusion (H.DIFF. + V.DIFF.). Units are degrees Celsius per year.

vective overturning, which is induced by this advective heating, cools the thick upper layer and counterbalances the heating. In the immediate vicinity of the Antarctic Continent, the heat balance of the 2 km thick upper oceanic layer is also maintained between the cooling by convective overturning and the advective heating by a weak and deep cell of meridional circulation (indicated by Fig. 7). The fluctuation of surface salinity induced by variable sea ice contributes to this overturning. In short, the efficient vertical spreading of heat by deep cells and associated convective overturning contribute to the slowdown of the CO_2-induced warming in the near-surface layer of the Circumpolar Ocean of the Southern Hemisphere.

Figure 18b indicates that the convective cooling of the upper 2 km ocean layer is less in S2X than in S1X, due partly to the slight increase of static stability in the upper ocean layer in the Circumpolar Ocean. Thus, the CO_2-induced reduction of convective cooling causes the very slow but significant warming of the subsurface

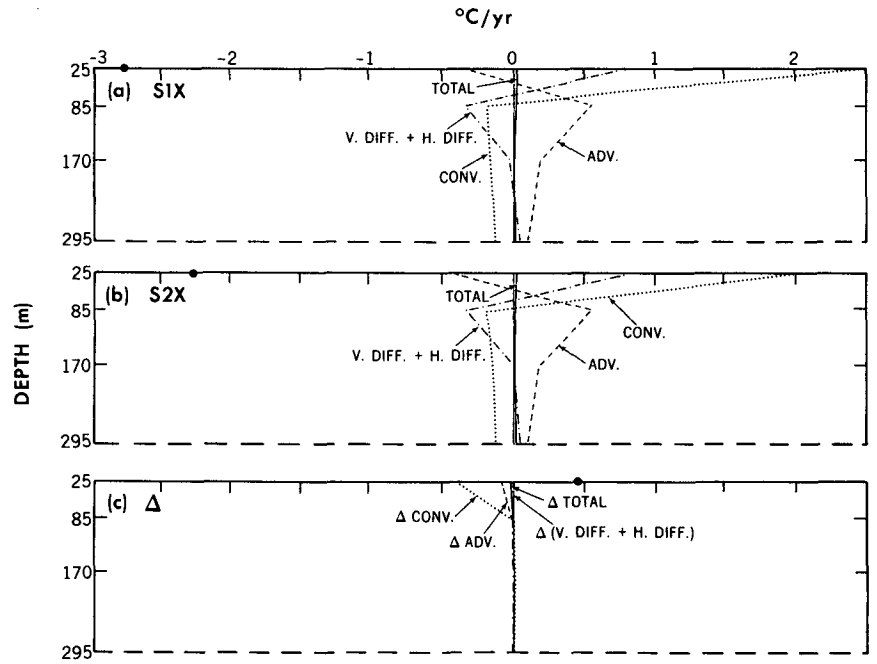

FIG. 19. As in Fig. 18, for the upper 295 m of the ocean for the synchronous integrations S1X (a) and S2X (b) and their difference S2X minus S1X (c).

ocean layer of the model, despite the reduced advective heating that results from the reduced poleward heat transport discussed earlier.

Although a slight warming of the sea surface is realized in the Circumpolar Ocean of the Southern Hemisphere during the early period of the experiment, the sea surface temperature is reduced with time during the last 15 year period, preventing the net warming of the sea surface during the 60 year period of the experiment. This result appears to suggest that, in addition to the efficient vertical homogenization of the upper ocean layer discussed above, other mechanisms exist that reduce the surface warming of the Circumpolar Ocean. To explore this issue, the analysis of the subsurface heat budget illustrated in Fig. 18 is repeated for the surface layers of the model ocean. Figures 19a and 19b show the vertical distributions of ADV, CONV, DIF and SQ from the S1X and S2X integrations, respectively. In addition, the differences of these terms between the two integrations are shown in Fig. 19c.

These figures indicate that, in both S1X and S2X integrations, the heat balance of the surface mixed layer in the Circumpolar Ocean is essentially maintained between the heating due to convection (i.e., CONV) plus diffusion (i.e., DIF) and the cooling due to the net melting of ice and snow and the heat exchange at the ocean surface (i.e., SQ). The surface heat loss due to the SQ term, however, is smaller in the S2X than the S1X integrations. On the other hand, the heat gain due to the CONV term is also smaller in the former than the latter. This is indicated by Fig. 19c, which illustrates the difference in each term between the two cases. Thus, the sea surface temperature difference between the two integrations hardly changes in the Circumpolar Ocean over the 60 year period.

The smaller convective heating of the mixed layer of the Circumpolar Ocean in the S2X integration is attributable to the increased stability of the halocline. As illustrated earlier by Fig. 13, the surface salinity difference between the S2X and S1X integrations is reduced slowly with time in the Circumpolar Ocean. The rate of the reduction becomes somewhat larger during the last 15 year period. This salinity reduction is essentially confined to the near surface layer of the model ocean, thereby suppressing the convective overturning of cold surface water by warmer deep water. This reduction of convective heating of the mixed layer helps prevent the warming of the Circumpolar Ocean surface despite the reduced heat loss from the surface.

The stabilization of the near surface layer of the Circumpolar Ocean in the S2X integration results mainly from the increased water supply to the oceanic surface. Figure 20a illustrates the latitudinal profiles of the zonal mean rates of water supply to the surface of the model ocean from the two integrations during the 50th to the 60th year period. The difference between the two rates is also shown in Fig. 20b in a magnified scale. Here the rate of surface water supply is defined as the net

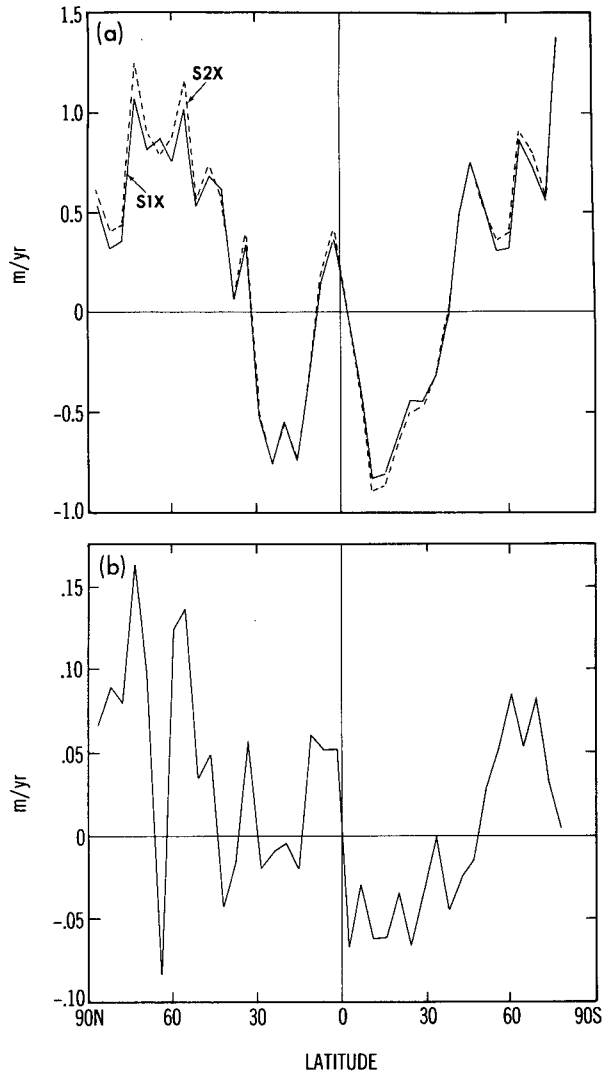

FIG. 20. Zonally averaged moisture fluxes (precipitation + runoff − evaporation) at the ocean surface averaged over the period 50 to 60 years: (a) S1X and S2X denote the synchronous integrations with normal and doubled atmospheric carbon dioxide, respectively; (b) the difference S2X minus S1X. The ordinate scale is 10 times larger in (b) than in (a). Units are meters per year.

downward surface water flux from precipitation, continental runoff, evaporation and sublimation. Figure 20b clearly indicates that the difference in surface water supply between the two integrations is positive poleward of 50°S latitude. As shown later in the subsection on the hydrologic cycle, the difference in precipitation rate increases in the Circumpolar Ocean because of the enhanced import of warm, moisture-rich air from the middle latitudes. On the other hand, the difference in evaporation rate between the two integrations is relatively small due to the absence of the CO_2-induced warming in this ocean. Thus, the surface water supply increases, thereby reducing the Circumpolar surface salinity in the S2X as compared with the S1X integration. In summary, the intensification of the surface

halocline, which results from the increased precipitation, weakens the convective mixing of surface water with the warmer subsurface water and prevents the net increase of the surface temperature in the Circumpolar Ocean. The process described above contributes to the slight reduction of sea surface temperature during the last 15 years of the experiment.

It is well known that the present model has a systematic bias toward transporting excessive water vapor into high latitudes. Thus, the intensification of the surface halocline mentioned above could be affected by such bias. Furthermore, the parameterization of the oceanic mixed layer in the present model is rather rudimentary. A careful reassessment of the surface halocline intensification should be made when these deficiencies of the model are resolved.

d. Atlantic Ocean

To evaluate the downward penetration of the thermal anomaly in the Atlantic Ocean towards the end of the experiment, the temperature difference between the S2X and S1X integrations, which is zonally averaged over the Atlantic Ocean, is time-averaged for the 50th–60th year period. The latitude–depth distribution of this difference thus averaged is shown in Fig. 21a and is compared with Fig. 21b, which illustrates the corresponding distribution for the Pacific Ocean of the model. The comparison between the two figures clearly indicates that the downward penetration of the warm anomaly in the 45°–75°N latitude belt is deeper in the Atlantic than the Pacific Ocean. The thermohaline circulation and accompanying convection are responsible for the deeper penetration of the thermal anomaly in the northern North Atlantic Ocean.

The streamfunctions of the North Atlantic thermohaline circulation obtained from both S1X and S2X integrations are time-averaged over the last 10 year period and are illustrated in Fig. 22. The difference between the two streamfunctions is also shown in the lower panel of Fig. 22. In the northern North Atlantic, the spacing between the contours of the streamfunction is widened from the S1X to the S2X experiments, indicating a substantial reduction in sinking. The reduction occurs gradually throughout the course of the experiment. Induced by the increased surface water flux, the surface salinity is reduced over the Arctic and surrounding oceans as noted in the preceding subsection. Such a salinity reduction increases the static stability of the upper ocean layer, thereby weakening the sinking in the northern North Atlantic as noted above. The surface salinity is reduced further due to the reduction in the advection of saline water from low latitudes.

The North Atlantic thermohaline circulation shown for the S1X integration in Fig. 22 is substantially weaker than the corresponding circulation in the equilibrium

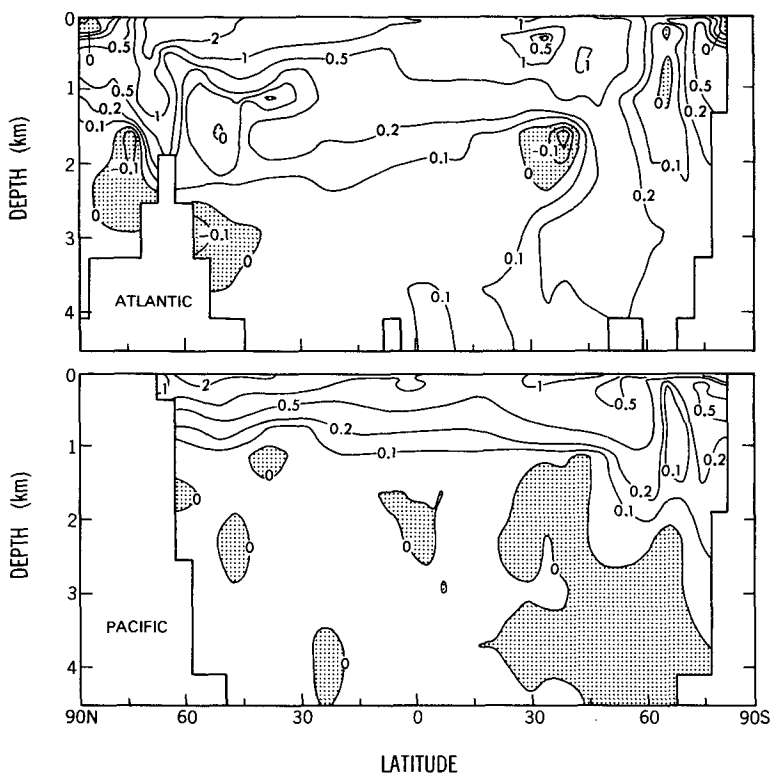

FIG. 21. Zonally averaged ocean temperature change (degrees Celsius) for the doubling of atmospheric carbon dioxide, averaged for the period 50 to 60 years of the synchronous integration: (top) for the Atlantic Ocean; (bottom) for the Pacific.

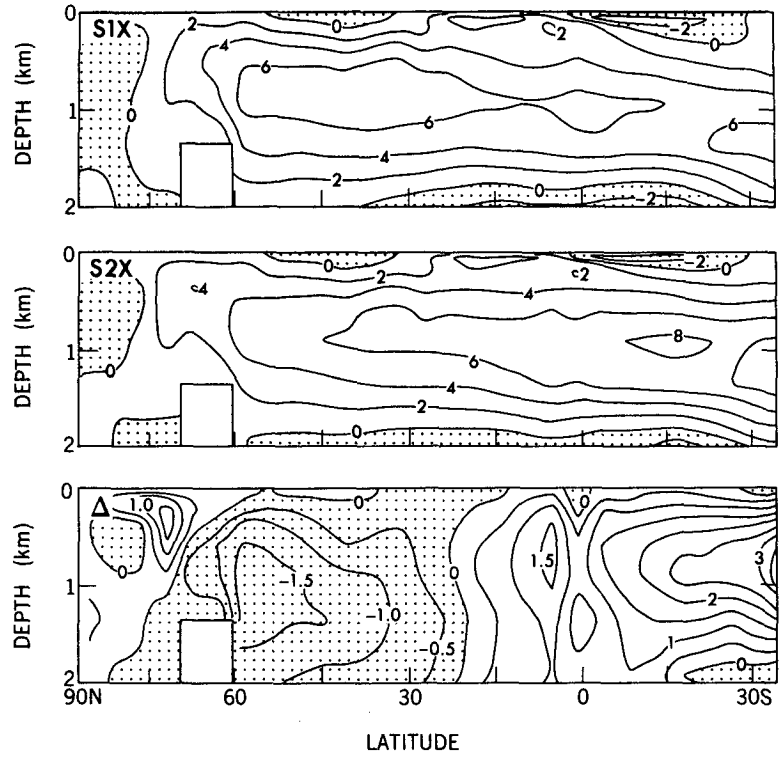

FIG. 22. Zonally integrated mass transport of the Atlantic Ocean for the synchronous integrations S1X (top panel) and S2X (middle panel) and their difference S2X minus S1X (bottom panel) for the period 50 to 60 years. Units are megatons per second.

state described in section 3b. During a preliminary synchronous integration, which originated from this equilibrium state, the intensity of the thermohaline circulation was weakened substantially with time. It appears that this weakening results from the "salt normalization" procedure that was continuously executed throughout the time integrations of the oceanic component of the model. The procedure adjusts the salinity by a constant value at all oceanic grid points such that the total salt in the model oceans remains unchanged. It was instituted in order to prevent a significant change in the total salt content of the oceans due to the long term accumulation of various computational inaccuracies, such as the truncation error involved in the time integrations of the prognostic equations of salinity and temperature. When this procedure is executed during the asynchronous integration in which the change in deep-water mass is accelerated, it slightly distorts the final equilibrium, thereby inducing a systematic trend during the synchronous integration which follows. The weakening trend was no longer evident during the (synchronous) S1X integration which followed the preliminary integration mentioned above. (See section 3a for the experimental procedures.) In evaluating the present experiment, it is therefore important to note that the North Atlantic thermohaline circulation is unrealistically weak in both S1X and S2X integrations because of the salt normalization procedure.

e. Hydrology

To evaluate how the hydrologic cycle of the model changed in response to the doubling of the atmospheric carbon dioxide, Figure 23 is constructed. The upper portion of this figure compares the latitudinal profile of the zonal mean precipitation rate $(\bar{P})^{\lambda}$ from the last 10 year period (i.e., 50 to 60th years) of the S1X and S2X integrations. The corresponding profile of zonal mean evaporation rate $(\bar{E})^{\lambda}$ is shown in the middle portion of the figure. In the bottom portion, the latitudinal profile of the difference in zonal mean precipitation rate between the two integrations and the corresponding profile for evaporation are shown in an expanded scale. As noted earlier, the differences computed here represent the total changes of $(\bar{P})^{\lambda}$ and $(\bar{E})^{\lambda}$ (over the 50 to 60th year period) which were realized in response to the abrupt doubling of atmospheric carbon dioxide.

Figure 23 shows that, in response to the CO_2 doubling, precipitation increased more than evaporation over the Arctic Ocean of the Northern Hemisphere and Circumpolar Ocean of the Southern Hemisphere where surface salinity is reduced during the course of the experiment. As noted already, the penetration of warm, moisture-rich air into higher latitudes in the warmer model atmosphere is responsible for the increase in the rate of precipitation in both polar regions.

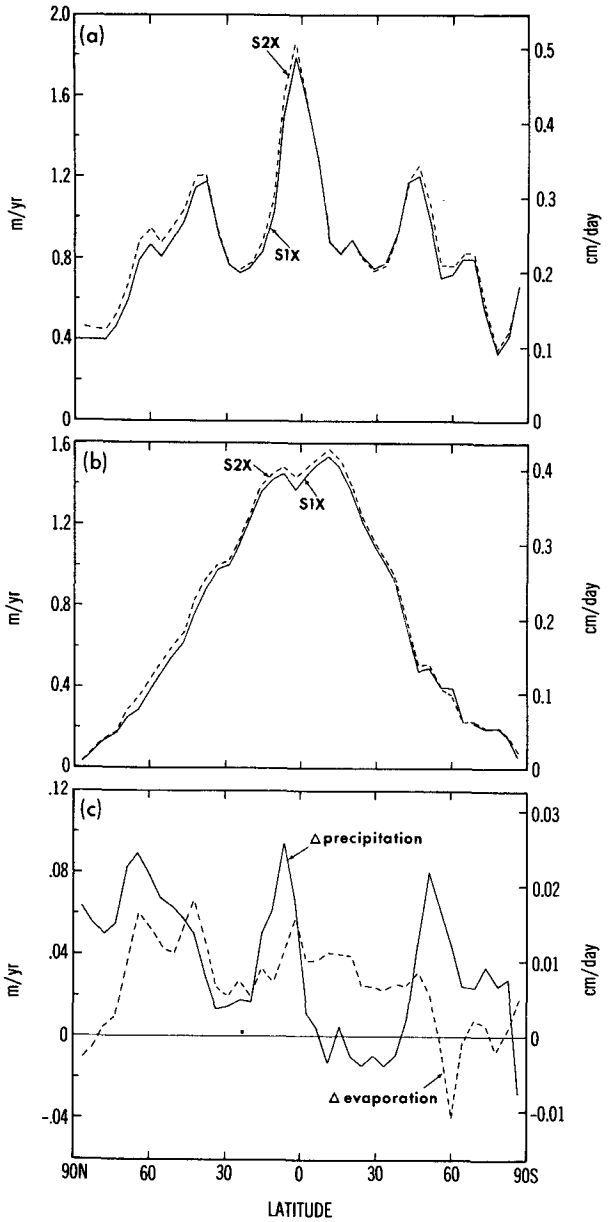

FIG. 23. Zonally averaged moisture fluxes from the atmospheric model. S1X and S2X denote the synchronous integrations with normal and doubled atmospheric carbon dioxide, respectively: (a) rate of precipitation; (b) rate of evaporation; (c) the difference S2X minus S1X. The ordinate scale is 10 times larger in (c). Units are meters per year on the left ordinate scale and centimeters per day on the right.

Over the Circumpolar Ocean of the Southern Hemisphere, the warming of the model troposphere is small but significant. However, no net warming of sea surface temperature is indicated there. Thus, the precipitation rate increased significantly, whereas evaporation failed to change substantially.

The changes in the rates of precipitation and evaporation, in turn, affect the rate of runoff from continents. Figure 24 illustrates the latitudinal profiles of zonal mean runoff averaged over the last 10 year period. In addition, the profile of the difference in runoff rate between the S2X and S1X integrations is also added to the lower half of the figure. As this figure indicates, the rate of runoff increases significantly over the Arctic Ocean and the surrounding regions.

In the model tropics, the zonal mean rate of precipitation increases to the north of the equator but is reduced to its south. The change of precipitation results from the interhemispheric asymmetry in the CO_2-induced change of sea surface temperature and is consistent with the corresponding change of meridional circulation, which is asymmetric relative to the equator and is discussed in the following subsection. The tropical change in $(\bar{P}^{\lambda} - \bar{E}^{\lambda})$, in turn, is responsible for the slight increase (reduction) of the zonal mean runoff to the north (south) of the equator, respectively. One should note, however, that the CO_2-induced change in tropical runoff is barely significant at the confidence level of 95% as indicated in Fig. 24.

f. Circulation

The doubling of atmospheric carbon dioxide not only changed the distributions of temperature and sa-

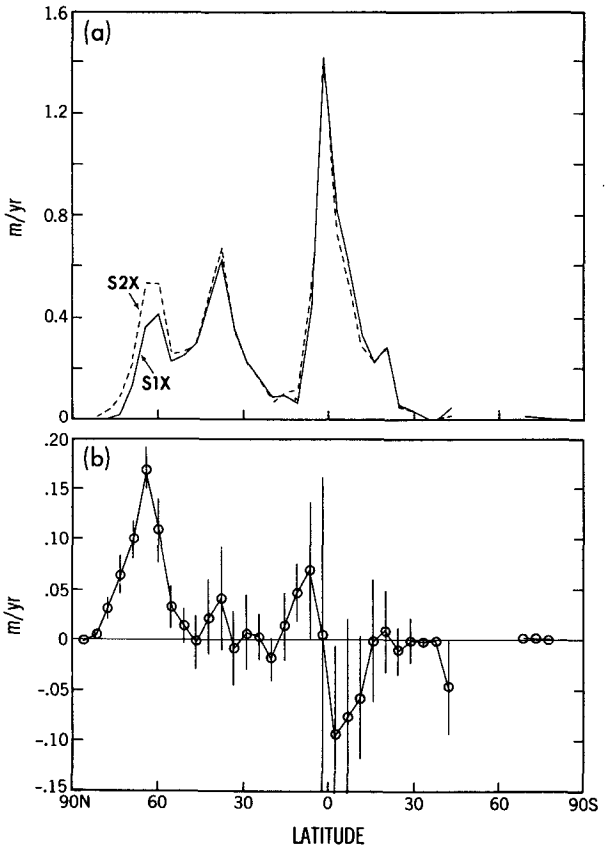

FIG. 24. Zonally averaged rate of water runoff (m yr^{-1}) from the continent to the ocean: (a) for the synchronous integrations with normal (S1X) and doubled (S2X) atmospheric carbon dioxide; (b) the difference S2X minus S1X, where the vertical bars indicate the 95% confidence intervals.

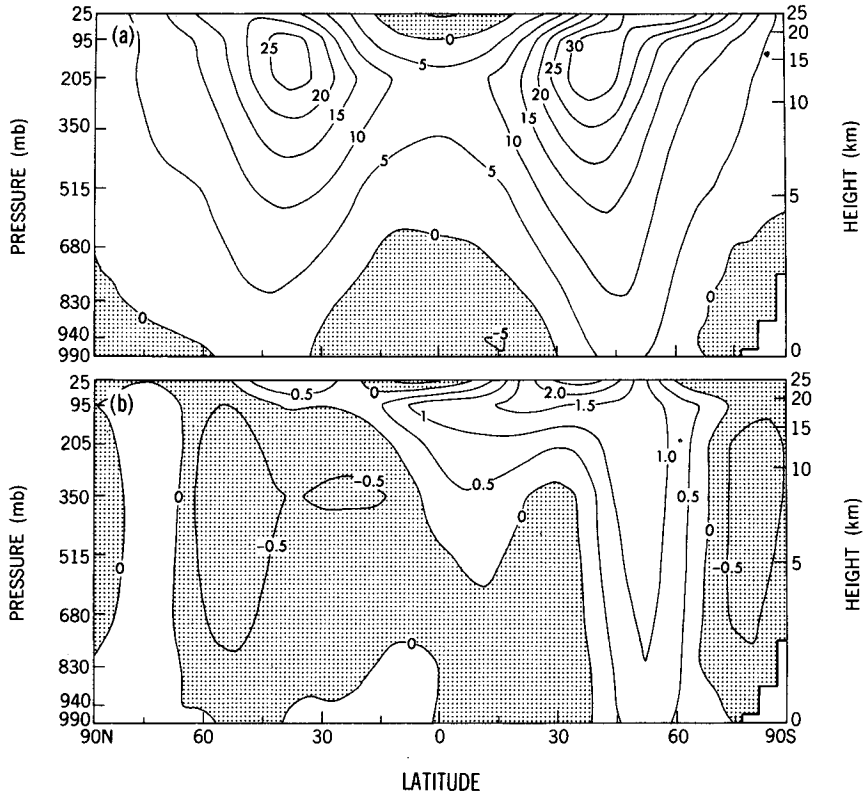

FIG. 25. Zonally averaged zonal wind in the atmosphere averaged over the period 50 to 60 years: (a) for the synchronous integration S1X; (b) the difference S2X minus S1X. Units are centimeters per second.

linity but also the general circulation of the coupled ocean–atmosphere model. Figure 25 illustrates the latitude–height distribution of zonal wind averaged over the 50 ~ 60th year period of the S1X integration. It also contains the distribution of the difference in zonal mean wind between the S2X and S1X integrations averaged over the same 10 year period. This figure indicates that, in the Southern Hemisphere of the model, westerlies intensified slightly during the 60 year period, responding to the general increase of meridional temperature gradient in the model troposphere. In the Northern Hemisphere where the meridional temperature gradient is reduced in the lower troposphere but increases in the upper troposphere, the westerlies are reduced slightly.

The change in zonal wind described above extends to the surface layer of the model troposphere, altering the latitudinal profile of surface wind stress at the ocean surface. This is indicated in Fig. 26, which shows the latitudinal profiles of zonal mean ocean surface wind stress from both S1X and S2X integrations and the profile of the difference between them during the last 10 year period of the experiment. In the Southern Hemisphere where the vertical wind shear and the baroclinicity increased, the magnitudes of both positive wind stress in middle latitudes and negative wind stress in the subtropics increased. On the other hand, the magnitude of wind stress became smaller in the Northern Hemisphere where the baroclinicity in the middle and lower model troposphere is reduced slightly.

In response to the doubling of atmospheric carbon dioxide, the meridional circulation also changed significantly in the coupled ocean–atmosphere system of the model. To examine the change, the latitude–height distribution of the difference in meridional circulation between the S2X and S1X integrations is illustrated in Fig. 27 by the streamfunction. As this figure indicates, the interhemispheric asymmetry in the CO_2-induced warming induced the change of tropical atmospheric circulation which sinks in the tropics of the Southern Hemisphere, crosses the equator near the surface, rises in the Northern Hemisphere tropics, and returns to the Southern Hemisphere in the upper model troposphere. The change in the cross-equatorial surface wind, in turn, alters the zonal wind and wind stress at the ocean surface of the model tropics (as indicated by Figs. 25 and 26) and induces the southward Ekman Drift of surface water across the equator and return subsurface flow as indicated in Fig. 27.

In middle and high latitudes of the Southern Hemisphere, both the indirect Ferrel Cell and the direct polar cell in the model atmosphere intensify, indicating the general increase of baroclinicity. In response to the increase of surface westerlies in middle latitudes, the Ek-

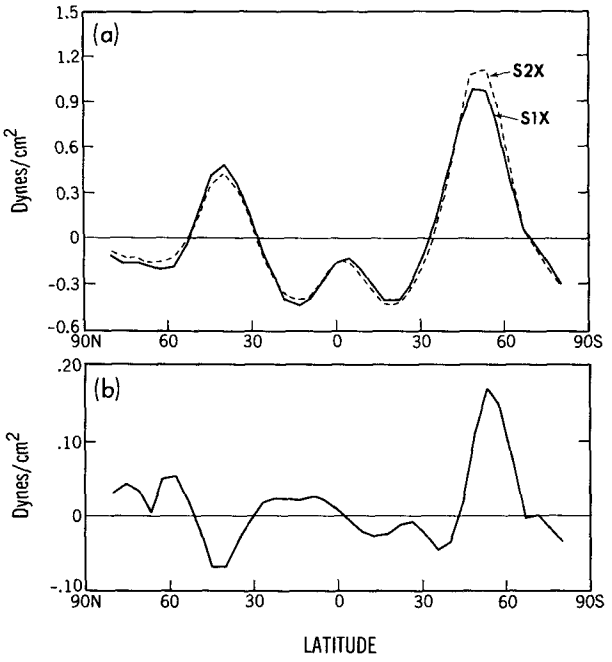

FIG. 26. Zonally averaged wind stress over the ocean surface: (a) for the synchronous integrations with normal (S1X) and doubled (S2X) atmospheric carbon dioxide for the period 50 to 60 years; (b) the difference S2X minus S1X, with the ordinate scale expanded. Units are dyn cm^{-2}.

man drift current intensifies, thereby increasing the northward advection of fresh surface water. Together with the increased surface water supply discussed earlier, this increased Ekman drift reduces surface salinity and stabilizes the surface layer, thereby preventing the warming of the Circumpolar Ocean surface as discussed earlier. The change in meridional circulation in the intermediate ocean layer of the Southern Hemisphere is mainly responsible for the reduction in the poleward heat transport mentioned in section 4b.

g. Feedback parameters

Before concluding this section, it is desirable to discuss briefly a possible bias in the transient response of climate simulated by the present model. To identify the most basic factors that control the transient response of climate, one can use the so-called zero-dimensional model of global climate proposed by Dickinson (1986). In his idealized model, the response of the global mean climate to a thermal forcing may be expressed by the following prognostic equation:

$$C\frac{dT'(t)}{dt} = \Delta Q - \lambda \cdot T'(t) \qquad (2)$$

where C is the effective heat capacity of the coupled ocean–atmosphere system, T' is the deviation of global mean surface air temperature from its equilibrium

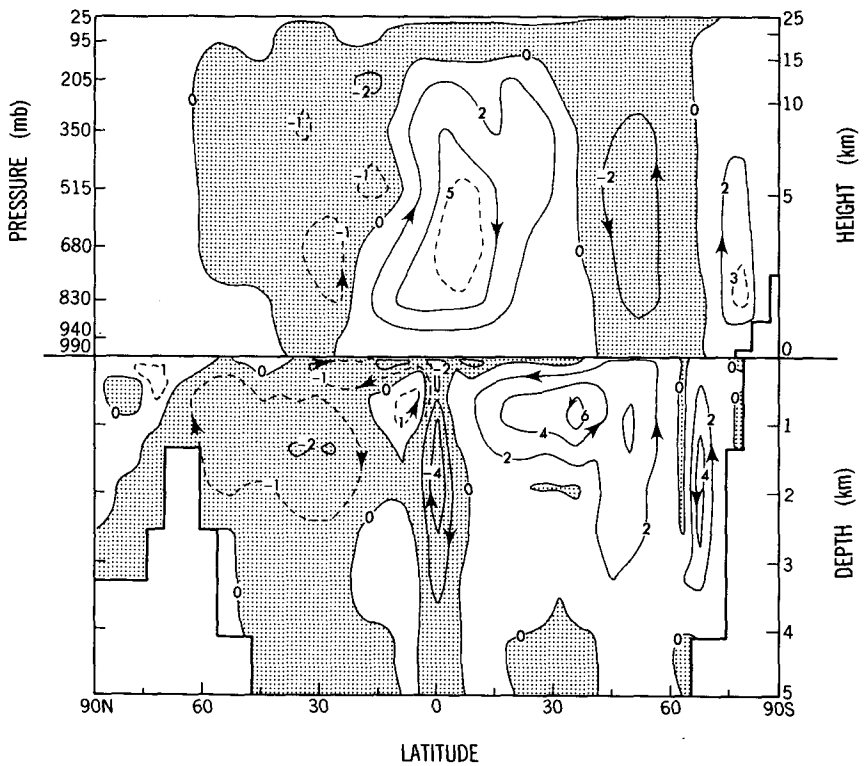

FIG. 27. Difference of the zonally integrated mass transport of the atmosphere and ocean between the synchronous integrations with doubled and normal atmospheric carbon dioxide for the period 50 to 60 years. Units are megatons per second.

value, t is the time elapsed after the abrupt doubling of atmospheric carbon dioxide, ΔQ is the radiative forcing exerted by the CO_2 doubling, and λ is the effective radiative damping coefficient of the system. Setting the right-hand side of Eq. (2) equal to zero, one can get the following expression for the equilibrium response T'_{eq} to the doubling of the atmospheric carbon dioxide:

$$T'_{eq} = \Delta Q/\lambda. \quad (3)$$

Equation (2) also implies that the time constant (τ) for the transient response is

$$\tau = C/\lambda. \quad (4)$$

For the coupled model used for the present study, the equilibrium response of the global mean surface air temperature to the doubling of atmospheric carbon dioxide is 2.4°C. This is a typical value for a model with prescribed cloud cover and is significantly smaller than the corresponding response of about 4°C from current models in which the distribution of cloud cover is predicted (Hansen et al. 1984; Wetherald and Manabe 1988). Because of the prescribed cloud cover, the coefficient of effective radiative damping is larger in the present model, making its equilibrium response smaller. Thus, the time constant of transient response τ is also shorter than other current models mentioned above.

In view of the fact that the current parameterization of the cloud feedback process is highly rudimentary, it has not been possible to determine which model has a more realistic rate of radiative damping. However, one should keep in mind that the time constant of the transient response of the present model lies in the shorter half of the current estimates. Thus, one should note that the delay in the response of the coupled model used here is relatively short.

Obviously, the behavior of the coupled model used for the present study is not as simple as that of the zero-dimensional model described here. In the coupled model, the effective heat capacity of the system increases with time as the CO_2-induced thermal anomaly penetrates downwards. Nevertheless, the analysis described here should be useful for evaluating the possible bias of the results obtained from the present experiment.

5. Summary and conclusions

The present study analyzes the transient response of a global ocean–atmosphere model with realistic geography to an abrupt doubling in the atmospheric concentration of carbon dioxide. It continues the earlier study of Bryan et al. (1988) conducted by use of a coupled model with a sector computational domain and an idealized geography. Confirming the results from the earlier study, the present analysis indicates that the transient response of the model climate to the CO_2 doubling exhibits a large interhemispheric asymmetry.

In the Northern Hemisphere, the CO_2-induced warming of the near surface atmosphere increases with increasing latitude and is most pronounced over the Arctic Ocean and its surroundings. The large increase of surface air temperature in high northern latitudes results from the poleward retreat of snow cover and sea ice with large surface albedo. In the upper layer of the model oceans, the CO_2-induced warming is at a maximum in the subpolar latitudes where the sea ice margin retreats polewards and surface albedo is reduced markedly. However, the warming becomes very small in the Arctic Ocean where sea ice insulates the near surface atmosphere from the underlying water with freezing temperature.

On the other hand, in middle and high latitudes of the Southern Hemisphere, the increase of surface air temperature is much slower than the Northern Hemisphere. To the south of 50°S latitude, no net increase of surface air temperature is indicated during the 60 year period of the experiment, in sharp contrast to the large warming in the corresponding latitudes in the Northern Hemisphere. Although the surface air temperature in the high southern latitudes increases slightly during the first 45 years of the experiment, it is reduced slightly with time during the last 15 years.

As suggested by Thompson and Schneider (1982), the slower rise of surface air temperature in the Southern Hemisphere is partly due to the larger thermal inertia of the ocean-dominated hemisphere. Furthermore, the efficient vertical mixing of heat over the 2-km thick upper ocean layer makes the effective thermal inertia particularly large in the Circumpolar Ocean of the Southern Hemisphere as discussed below.

Owing to the absence of a meridional barrier at the latitudes of the Drake Passage, a deep wind-driven cell of meridional circulation is maintained in the Circumpolar Ocean of the model. In addition, a deep reverse cell develops in the immediate vicinity of the Antarctic Continent. The thermal advection by these cells and associated convective overturning results in the very effective mixing of heat over a very thick upper ocean layer and increases the effective thermal inertia of the ocean, thereby contributing to the slowdown of the CO_2-induced warming in the near surface layer of the Circumpolar Ocean.

There is an additional mechanism that prevents the increase of the surface temperature in the Circumpolar Ocean. The increase of precipitation due to the enhanced penetration of warm, moisture-rich air aloft into high latitudes reduces the surface salinity, increases the static stability of the near surface ocean layer and suppresses the convective exchange of heat between the surface layer and the warmer underlying layer, contributing to the cooling of the surface layer. This accounts for the cooling of the sea surface and overlying air during the last 15 year period of the experiment.

Accompanied by the temperature change described above, the general circulation in the coupled system also undergoes changes, which are asymmetric relative to the equator. For example, in response to the CO_2 doubling, the westerlies in middle latitudes are reduced very slightly in the Northern Hemisphere whereas they increased slightly in the Southern Hemisphere. The intensification of surface westerlies in middle latitudes of the Southern Hemisphere results in the slight intensification of the northward Ekman drift currents as part of a deep, wind-driven cell of meridional circulation in the Circumpolar Ocean of the Southern Hemisphere.

The interhemispheric asymmetry of temperature change induces a change in atmospheric meridional circulation with rising and sinking motion in the tropics of the Northern and Southern hemispheres, respectively. Although they are small, the tropical changes in the rates of precipitation and runoff are also asymmetric relative to the equator. They are positive to the north of the equator and are negative to its south.

Although the present study deals with the response of the coupled model to an abrupt doubling of atmospheric carbon dioxide, it is likely that the deep well-mixed column of water also prevents the Subantarctic sea surface temperature from rising in the case of a more probable, gradual CO_2 increase. In order to confirm this speculation, a time integration of 200 years[1] was recently conducted imposing a gradual increase of CO_2 at the rate of 0.8% per year beginning from the year 1950 AD. Given this rate of increase, a doubling of atmospheric CO_2 occurs after 87 years, i.e., around the year 2037 AD. Such an increase is inside the range of the projections for the CO_2 equivalent effect of all greenhouse gases. It was found that in high latitudes of the Southern Hemisphere the surface air temperature fails to increase significantly even after 200 years of the integration during which the CO_2 concentration increased by a factor of more than 4. This result suggests that it takes a very long time before the deep water warms up enough to significantly raise the surface temperature of the Circumpolar Ocean of the Southern Hemisphere.

Broecker (1987) suggested that the thermohaline circulation in the North Atlantic Ocean may collapse in response to the future increase of atmospheric carbon dioxide. In a CO_2-rich atmosphere, warm and moist air penetrates into higher latitudes and increases the excess of precipitation over evaporation as indicated in Fig. 20. The increased supply of freshwater at the ocean surface in high latitudes may reduce the surface salinity and intensify the halocline in the Arctic and northern North Atlantic Ocean. This, in turn, can prevent the formation of deep water because of the stable stratification in the upper layer and cause the collapse of the thermohaline circulation in the Atlantic Ocean. Although such a collapse did not materialize during the course of the present experiment, the sinking in the northern North Atlantic is reduced substantially. The overall intensity of the thermohaline circulation in the North Atlantic is weakened only slightly.

It should be noted here that the intensity of thermohaline circulation in the Atlantic Ocean of the present model is unrealistically weak for the reason discussed in section 4d. Recently, Stouffer et al. (1989) investigated the climatic response to a gradual increase of atmospheric carbon dioxide (1%/yr) by use of a coupled model which has seasonal variation of insolation and the thermohaline circulation has realistic intensity. During the 100 year period of the experiment, substantial weakening (30% reduction after 65 years) of the Atlantic thermohaline circulation was noted through the mechanism similar to that described in the preceding paragraph. Due to the reduced northward advection of warm surface water and the strong vertical convective mixing, the increase of surface air temperature was relatively small over the northern North Atlantic in their experiment. Washington and Meehl (1989) noted a CO_2-induced weakening of thermohaline circulation in the North Atlantic Ocean in a recent numerical experiment conducted with their coupled model, although the circulation has some unrealistic features with its sinking branch in middle latitudes.

Mercer (1978) speculated that the West Antarctic Ice Sheet, resting upon bedrock below sea level, may be subject to rapid shrinkage and disintegration under the impact of the CO_2-induced climate change. Bentley (1983) suggested that the basal melting of the Ross and Filchne-Ronne ice shelves may be accelerated by the intrusion of warmer sea water, making them thinner and unpinned from the bedrock and eventually accelerating the calving of the ice sheet. In the present experiment, the sea surface fails to warm up and sea ice thickness even increases slightly off the Antarctic Coast during the 60 year period of the experiment. This result suggests that the collapse of the West Antarctic Ice Sheet may be a very remote possibility. However, the occurrence of the small but significant subsurface warming of up to 0.5°C prevents one from completely eliminating the possibility of the basal melting of ice shelves and eventual collapse of the ice sheet.

The result from the present study is in contrast to the results of Schlesinger et al. (1985) and Washington and Meehl (1989). For example, Schlesinger et al. obtained a nearly symmetric response to an abrupt dou-

[1] For the economy of computation, this 200 year integration of the oceanic component of the model was performed concurrently with 40-years integration of the atmospheric component. Since the time scale of thermal adjustment for the model atmosphere is much shorter than the time scale for the global warming of sea surface temperature, it is expected that this asynchronous coupling should not alter significantly the rate of the general warming of the model climate. In this asynchronous integration, no attempt was made to accelerate the thermal evolution of the deep ocean as described in section 3.

bling of atmospheric carbon dioxide by use of a global model with seasonal variation of insolation and prescribed distribution of salinity at the sea surface. Washington and Meehl (1989) recently conducted a similar experiment by use of a global model with predicted salinity. Although their results indicate slightly smaller warming in high latitudes of the Southern Hemisphere compared to that of the Northern Hemisphere, this feature is much less pronounced than the present result. The initial conditions for these experiments are determined based upon observations, thereby allowing a significant climatic drift caused by the biases of these models. On the other hand, a quasi-equilibrium climate from an asynchronous integration is used as the initial condition for the present experiment. Both of the models used in these studies have seasonal variation of insolation, whereas the present model does not. Therefore, it is not a trivial matter to determine the basic causes for the difference between these and the present results. Nevertheless, the discrepancy may result from the fact that the surface westerlies and wind-driven cell in the Circumpolar Ocean of their models are much weaker than those simulated in the present study. A critical assessment of this discrepancy is a subject for future research.

One important simplification of the present model is the elimination of the seasonal variation of insolation. This simplification may affect the rate of deep water formation, thereby affecting quantitatively the transient response of the model. Nevertheless, it is not likely that the seasonal forcing prevents the efficient vertical mixing of water in the Circumpolar Ocean discussed in this study and allows the sea surface temperature to rise in high latitudes of the Southern Hemisphere. The seasonal variations of sea ice and surface salinity may also weaken the halocline by inducing convective overturning, preventing the cooling of the Circumpolar Ocean surface which occurred towards the end of the present experiment. However, it is reassuring that the response of a seasonal model to gradually increasing CO_2 indicates that sea surface temperature in the Circumpolar Ocean poleward of 45°S fails to rise significantly during the course of the 100-year experiment (Stouffer et al. 1989).

Acknowledgments. We wish to thank Ron Stouffer and Keith Dixon for their assistance in the modeling and analysis of the coupled ocean–atmosphere model. The constructive reviews by Stanley Jacobs of the Lamont-Doherty Geological Observatory and by George Mellor and Ron Stouffer were very helpful for improving the manuscript. Special thanks are extended to GFDL staff members Phil Tunison, Cathy Raphael, Jeff Varanyak and John Conner for their help in preparation of the figures and Joyce Kennedy and Wendy Marshall for typing the manuscript. Jerry Mahlman, Director of the Geophysical Fluid Dynamics Laboratory, has encouraged and supported this project and generously allocated the computer resources needed for the computations.

REFERENCES

Bentley, C. R., 1983: West Antarctic ice sheet: diagnosis and prognosis. Proceedings: CO_2 Research Conference: Carbon dioxide, Science and Consensus, IV 3-50, Conf-820970, 19–23 Sep. 1982, U.S. Dept. of Energy, Washington, DC.

Broccoli, A. J., and S. Manabe, 1987: The influence of continental ice, atmospheric CO_2, and land albedo on the climate of the last glacial maximum. *Climate Dyn.*, **1,** 87–99.

Broecker, W. S., 1987: Unpleasant surprises in the greenhouse? *Nature,* **329,** 123–126.

Bryan, K., 1969: Climate and the ocean circulatin: III. The ocean model. *Mon. Wea. Rev.*, **97,** 806–827.

——, 1982: Poleward heat transport by the ocean. *Ann. Rev. Earth Planet. Sci.*, **10,** 15–38.

——, 1984: Accelerating the convergence to equilibrium of ocean–climate models. *J. Phys. Oceanogr.*, **14,** 666–673.

——, and L. J. Lewis, 1979: A water mass model of the world ocean. *J. Geophys. Res.*, **84**(C5), 2503–2517.

——, and M. J. Spelman, 1985: The ocean's response to a CO_2-induced warming. *J. Geophys. Res.*, **90,** 11679–11688.

——, S. Manabe and R. C. Pacanowski, 1975: A global ocean–atmosphere climate model. II: The oceanic circulation. *J. Phys. Oceanogr.*, **5,** 30–46.

——, F. G. Komro, S. Manabe and M. J. Spelman, 1982: Transient climate response to increasing atmospheric carbon dioxide. *Science,* **215,** 56–58.

——, S. Manabe and M. J. Spelman, 1988: Interhemispheric asymmetry in the transient response of a coupled ocean-atmospheric model to a CO_2 forcing. *J. Phys. Oceanogr.*, **18,** 851–867.

Cess, R. D., and S. D. Goldenberg, 1981: The effect of ocean heat capacity upon global warming due to increased atmospheric carbon dioxide. *J. Geophys. Res.*, **86,** 498–502.

Crutcher, H. L., and J. M. Merserve, 1970: *Selected Level Heights, Temperature, and Dew Points for the Northern Hemisphere.* NAVAIR 50-1C-52, U.S. Naval Weather Service, Washington, DC.

Deacon, G. E. R., 1937: Note on the dynamics of the southern ocean. *Discovery Reports,* Cambridge University Press, **15,** 125–152.

Dickinson, R. E., 1986: *Climate Change, and Ecosystems.* B. Bolin, B. R. Doos, J. Jager and R. A. Warrick, Eds. Wiley & Sons, Chichester, Scope 29, 207–270.

Gill, A. E., and K. Bryan, 1971: Effects of geometry on the circulation of a three dimensional Southern Hemisphere ocean model. *Deep-Sea Res.*, **18,** 685–721.

Gordon, C. T., and W. Stern, 1982: A description of the GFDL global spectral model. *Mon. Wea. Rev.*, **110,** 625–644.

Hansen, J., A. Lacis, D. Rind, G. Russell and P. Stone, 1984: Climate Sensitivity: Analysis of feedback mechanisms. *Climate Processes and Climate Sensitivity, Geophys. Monogr., 29,* Maurice Ewing, Vol. 5, J. E. Hansen and T. Takahashi, Eds. AGU 130–163.

Hoffert, M. K., A. J. Callegari and C.-T. Hsieh, 1980: The role of deep sea storage in the secular response to climate forcing. *J. Geophys. Res.*, **85,** 6667–6679.

Levitus, S., 1982: *Climatological Atlas of the World Ocean,* NOAA Prof. Paper No. 13, U.S. Dept. of Commerce, Washington, DC, 173 pp.

London, J., 1957: A study of the atmospheric heat balance. Final Report, Contract AF19(122)-165, Dept. Meteor. Oceanogr., New York University, 99 pp.

Manabe, S., 1969: Climate and the ocean circulation: I. The atmospheric circulation and the hydrology of the earth's surface. *Mon. Wea. Rev.*, **97,** 739–774.

——, and K. Bryan, 1969: Climate calculations with a combined ocean–atmosphere model. *J. Atmos. Sci.*, **26,** 786–789.

——, and R. T. Wetherald, 1985: CO_2 and hydrology. *Advances in Geophysics,* Vol. 28A, pp. 131–157, Academic Press.

——, and R. J. Stouffer, 1988: Two stable equilibria of a coupled ocean–atmosphere model. *J. Climate,* **1,** 841–866.

——, J. Smagorinsky and R. F. Strickler, 1965: Simulated climatology of a general circulation model with a hydrologic cycle. *Mon. Wea. Rev.,* **93,** 769–798.

Mercer, J. H., 1978: West Antarctic ice sheet and CO_2 greenhouse effect, a threat of disaster. *Nature,* **271,** 321–325.

Oeschger, H., H. Siegenthalaer, U. Schotterer and A. Gugelman, 1975: A box diffusion model to study the carbon dioxide exchange in nature. *Tellus,* **27,** 168–192.

Oort, A. H., and T. H. Vonder Haar, 1976: On the observed annual cycle in the ocean-atmosphere heat balance over the Northern Hemisphere. *J. Phys. Oceanogr.,* **6,** 781–800.

Posey, J. W., and P. F. Clapp, 1964: Global distribution of normal surface albedo. *Geofis. Int.,* **4,** 33–48.

Sasamori, T., J. London and D. V. Hoyt, 1972: Radiation budget of the Southern Hemisphere. *Meteorological Monograph,* Vol. 13, C. W. Newton, Ed. Amer. Meteor. Soc., 9–22.

Schlesinger, M. E., W. L. Gates and Y. J. Han, 1985: The role of the ocean in CO_2-induced climatic warming: Preliminary results from the OSU coupled atmosphere-ocean GCM. *Coupled Ocean-Atmosphere Models,* J. C. J. Nihoul, Ed., pp. 447–478, Elsevier.

Semtner, A. J., and R. M. Chervin, 1988: A simulation of the global ocean circulation with resolved eddies. *J. Geophys. Res.,* **93,** 15 502–15 522.

Spelman, M. J., and S. Manabe, 1984: Influence of oceanic heat transport upon the sensitivity of a model climate. *J. Geophys. Res.,* **89,** 571–586.

Stouffer, R. J., S. Manabe and K. Bryan, 1989: Interhemispheric asymmetry in climate response to a gradual increase of atmospheric CO_2. . *Nature,* **342,** 660–662.

Sverdrup, H. U., M. W. Johonson and R. H. Fleming, 1942: *The Oceans: Their Physics, Chemistry, and General Biology.* Prentice Hall, 1087 pp.

Taljaard, J. J., H. van Loon, H. L. Crutcher and R. L. Jenne, 1969: *Climate of the Upper Air, Part I: Southern Hemisphere, Vol. 1, Temperatures, Dew Points, and Heights at Selected Pressure Levels,* NAVAIR 50-IC-55, U.S. Naval Weather Service, Washington, DC.

Thompson, S. L., and S. H. Schneider, 1982: Carbon dioxide and climate: The importance of realistic geography in estimating the transient temperature response. *Science,* **217,** 1031–1033.

Washington, W. M., and G. A. Meehl, 1989: Climate sensitivity due to increased CO_2: Experiments with a coupled atmosphere and ocean general circulation model. *Climate Dyn.,* **4,** 1–38.

Wetherald, R. T., and S. Manabe, 1988: Cloud feedback processes in a general circulation model. *J. Atmos. Sci.,* **45,** 1397–1415.